Ligand Based Pharmacophore Modeling, Virtual Screening, Molecular Docking, Molecular Dynamic simulation and In-silico ADMET Studies for the Discovery of Potential BACE-1 Inhibitors

Usman Shareef (✉ usman.scps@stmu.edu.pk)

  Shifa College of Pharmaceutical Sciences, Shifa Tameer-e-Millat University

Aisha Altaf

  Shifa College of Pharmaceutical Sciences, Shifa Tameer-e-Millat University

Muhammad Kazim Zargaham

  Shifa College of Pharmaceutical Sciences, Shifa Tameer-e-Millat University

Rohail Bhatti

  Drexel University College of Medicine

Ahsan Ibrahim

  Shifa College of Pharmaceutical Sciences, Shifa Tameer-e-Millat University

Muhammad Ammar Zahid

  Qatar University 9FJJ+7QG

Research Article

Abstract

Pharmacophore modeling is an innovative technology to explore and extract potential interactions between ligand-protein complexes. On the other hand, virtual screening is an in-silico technique that uses pharmacophore models to analyze extensive databases of compounds or approved drugs to evaluate interactions. These techniques enable to discover, establish, and evaluate therapeutics and other biologically active compounds and also allow the optimization of several hundred and thousand compounds to be tested for interaction against the target protein or receptor, which narrows down the potential molecules that can be used for further studies. Drug repurposing can be done by integrating these techniques into the study design, allowing reduced cost associated with conventional hit and trial testing of compounds, running large databases in shorter duration. The study reported the successful generation and validation of pharmacophore model with subsequent virtual screening. Virtual screening of databases produced 6 hits which were further subjected to *in-silico* analysis and resulted in identification of anileridine as the potential BACE-1 inhibitor. Anileridine showed significant interaction with one of the important amino acids of the catalytic dyad of the enzyme i.e. Asp32. Furthermore, MD simulations supported the molecular docking and MM-GBSA results and revealed to formation of stable interactions between anileridine and BACE-1. After establishing anileridine as the potential BACE-1 inhibitor procured from already approved drugs, it was subjected to extensive *in-silico* ADMET studies. Furthermore, the model (AHRRR) can be used to rationally design novel inhibitors of BACE-1 and also identify new molecules from databases as potential BACE-1 inhibitors.

Introduction

Alzheimer's disease (AD) is a chronic and progressive neurodegenerative disease characterized by cognitive dysfunction impacting speech, memory, reasoning, and comprehension, usually affecting the population above the age of 65 years [1] [2]. The most significant pathological changes in the diseased state include neuritic plaques and neurofibrillary tangles, associated with the buildup and overproduction of amyloid-beta peptide (Aβ) [3]. The earliest hallmark in the disease process is the accumulation of Aβ, cognitive impairment, and clinical symptoms of memory loss or dementia start to appear 10–20 years later [4]. The metabolism and homeostasis of Aβ are regulated by the enzyme BACE1 (β-secretase 1), which cleaves amyloid precursor protein (APP) to form Aβ; this enzyme acts as an avenue for the therapeutic intervention to regulate the pathological progression of AD at early stages. However, the BACE1 inhibition is critical such that it is to be controlled at a certain level so that the regular physiological activity of the enzyme is balanced [5].

AD is a major cause of dementia and the fifth leading cause of death in the population above the age of 65 years, and it has a substantial economic burden with the overall global cost for the management of Alzheimer's disease and related dementias (ADRDs) during the year 2019 was 2.8 trillion USD and is expected to reach up to 11.3 trillion–27.3 trillion USD by 2050. The cost includes direct healthcare management, including nursing care, hospice care, and healthcare, and indirect attributions to improve quality of life and provide a supportive environment to family and patients[6–8]. This economic and

societal burden of AD is expected to increase as the population ages, opening the window to look for new therapeutic targets for the management of disease progression to delay the clinical symptoms of dementia and cognitive impairment, which could improve the quality of life of people with AD.

In affluent nations, it is the sixth-largest cause of death and the most prevalent cause of dementia. The likelihood of dementia has increased in developing countries such as Pakistan as a result of the country's rising life expectancy. Pakistan, the sixth-most populous nation in the world, is thought to have between 150,000 and 200,000 dementia cases [9].

Recently, attention has been focused on an approach called 'drug repurposing' due to the rising high cost of drug discovery and development and extensive and strict regulation during clinical development. The drug repurposing (drug repositioning, re-profiling, or re-tasking) approach investigates the application of already approved drugs and investigational drugs beyond the primary scope or indication [10]. Drug repurposing offers the advantage of reduced cost, accelerated development timeline, and lower risk of failure as the drug has already proven safe in clinical and pre-clinical data [11]. Several approaches can drive drug repurposing; pharmacophore modeling and virtual screening serve this purpose, where pharmacophore refers to the part of a chemical structure responsible for eliciting the biological response [12].

Pharmacophore modeling is an innovative technology to explore and extract potential interactions between a drug or ligand and a target protein complex [13]. On the other hand, virtual screening is an in-silico technique that uses pharmacophore models to analyze extensive databases of compounds or approved drugs to evaluate their potentials for different diseases [14]. These techniques enable to discover, establish, and evaluate therapeutics and other biologically active compounds[15] and also allow the optimization of several hundred and thousand compounds to be tested for interaction against the target protein or receptor, which narrows down the potential molecules that can be used for further studies[16]. Drug repurposing can be done by integrating these techniques into the study design, allowing reduced cost associated with conventional hit and trial testing of compounds, running large databases in shorter duration, and targeting flexibility as pharmacophore can be tailored and modified [17].

Correlating this with Alzheimer's disease in the present study, a pharmacophore model AHRRR was established for the identification of significant pharmacophore features using BACE-I inhibitors gathered from the ChEMbL database. The core and primary objective the study was to re-evaluate already approved drugs to discover potential BACE-1 inhibitors as well as to identify new compounds from a diversity database whose biological activities have not been evaluated yet.

Structure of BACE-1 enzyme:

BACE-1 enzyme belongs to the family of aspartic proteinases and causes the proteolytic cleavage of the amyloid precursor protein leading to the production of amyloid beta peptides in brain parenchyma [18]. BACE-1 is more than 30 percent homologous to the pepsin family members of proteases having two of

the conserved regions as active domains. BACE-1 also has structural homology with other aspartyl proteases such as cathepsin D, BACE-2, renin and cathepsin E.

BACE-1 enzyme is composed of 501 amino acids with overall five essential domains, the signal peptide domain, pro-peptide domain, catalytic domain, transmembrane domain and cytosolic domain. The signal peptide domain of BACE-1 transports it to the endoplasmic reticulum where the cleavage of pro-peptide domain occurs by furin protease. Later on, the transmembrane domain causes the translocation of the protein into the Golgi complex leading to posttranslational processing and complete maturation of BACE-1 enzyme. The transmembrane domain mediates the anchorage of BACE-1 with the plasma membrane. The catalytic domain contains the active aspartic residues of BACE-1 enzyme [19].

BACE-1 has a sizable active site that is made up of numerous subsites, called pockets. The hydrophobic pockets S1 and S3 are adjacent to one another. These pockets contain the residues Leu30, Phe108, Ile110, Ile118, and Trp115. The S2 and S4 pockets possess hydrophilic amino acid residues including Lys9, Ser10, Thr72, Gln73, Thr231, Thr232, Arg235, Arg307, and Lys321. The subsites S3' and S4' are solvent exposed and contain residues like Pro70, Thr72, Glu125, Arg128, Agr195, and Trp197. The S2' subsite is comprised of residues such as Ser35, Val69, Tyr71, Ile126, and Tyr198. All of these residues are hydrophobic and amphiphilic. S1' subsite contains the major catalytic residues Asp 32 and Asp 228, along with Ile 226 and Val 332 residues that are hydrophobic in nature[20].

The extracellular portion of BACE-1 contains the active amino acid residues Asp 32 and Asp 228. Several molecular docking analyses have revealed the interaction of these catalytic aspartates with a wide range of BACE-1 inhibitors [21–23]. The 3D crystal structure of BACE-1 PDB ID: 7MYI and its docked inhibitor are shown in Fig. 2.

After studying the earliest inhibitor of BACE-1 i.e. OM99-2, the structure elucidation of BACE-1 showed that the active site was consisted of 28 amino acid residues as the ligand binding pocket, with sub-pockets: S1, S2, S3, S4, S1', S2', S3', and S4'[25]. Within the N-terminal lobe, the active site of BACE-1 had a shield over it in the form of β-hairpin loop, located in between Val67 and Glu77, which is the flexible portion of the active site and regulates the access of substrate or ligand to the active site [26]. The amino acid residues on the flap determine the closed and open conformation of BACE-1. Tyr 71 residue forms a hydrogen bond with Trp 76 leading to a closed conformation of BACE-1, while the absentia of hydrogen bond between Tyr 71 and Trp 76 will lead to an open conformation of BACE-1, with no physical separation between the S1 and S2' sub-pockets[27].

Another important component of the BACE-1 active site is the 10 seconds loop, which is present along with Ser 10 residue, within the S3 binding pocket. Most substrates can attach and interact with the S3 pocket when the 10 second loop adopts an open conformation. Hence, when a ligand binds the binding pocket of BACE-1, this causes the β-hairpin loop to close and maximum interaction between the ligand and the 10 second loop. The water molecule located in the center of the binding pocket plays a significant role in the hydrolysis of the peptide bonds of BACE-1 substrates [26].

Material and Methods

Procurement and processing of dataset:

The BACE-1 inhibitors were taken from ChEMbL database, which is an open source database containing information regarding several parameters such as binding, functional and ADMET for a large number of structurally diverse chemical entities [28]. The target protein human BACE-1 (β-Secretase, ChEMbL4822, UniProt Accession No: p56817) was selected and a total of 10,511 BACE-1 inhibitors were procured on the basis of known IC_{50} bioactivity. The dataset was further processed by applying the filters such as zero Lipinski violations, single protein format assays and known pChEMbL values. After applying the filters the compounds were reduced to 2570. The Tab Separated Values (TSV) file was downloaded which consisted of information regarding SMILES, IC_{50} in nM, pChEMbL, ALogP, molecular weight (Mol.Wt) and assay format and description. The SMILES format was converted to 3D SDF format using an online tool called Online SMILES Translator (https://cactus.nci.nih.gov/translate/).

Scaffold Decomposition:

The dataset obtained from ChEMbL database was further subjected to Scaffold decomposition using Schrödinger Suite Maestro [29] in order to identify the common scaffolds and group the compounds into classes on the basis of number of rings or number of ring systems [30, 31]. Several different scaffolds were obtained and arranged according to number of ring systems and the compounds were grouped together in scaffolds according to their pChEMbL values. The scaffold (S)-5-(3-(pyridin-3-yl)phenyl)-3,5-dihydro-4H-imidazol-4-one consisting of 51 source structures was chosen for further processing. The chemical structure of the scaffold is shown in Fig. 3.

Preparation of training set and test set:

The 51 molecules obtained after the selection of the specific scaffold were further divided into training set and test set for the purpose of generating and validating pharmacophore model. The compounds were randomly divided into both sets using 70:30 respectively. 36 molecules were randomly allocated to the training set while test set contained 15 molecules. Afterwards, inhibitors in both sets were processed using LIGPREP [32] with EPIK [33] in order to expand the tautomeric and protonation states of all the molecules at physiological pH 7.0 ± 2 followed by the application of OPLS4 (optimized potential for liquid simulations) force field for the energy minimization using default parameters [34]. Additionally, conformers for each compound were created utilizing the create phase database wizard's conformer creation option.

Generation of Pharmacophore model:

The pharmacophore was created using the Schrödinger package's PHASE module [35, 36]. In essence, the pharmacophore gives information on the minimal structural requirements needed to bind to the target

protein [37]. The ligand-based approach was used for the generation of pharmacophore model(s) using the training set database and 7.2 pChEMbL values as a threshold value for the active compounds. The compounds having pChEMbL value of ≥ 7.2 were deemed active and 7.2 pChEMbL values were deemed inactive. The six built-in pharmacophore characteristics provided by PHASE are the aromatic ring (R), positively ionizable (P), negatively ionizable (N), hydrogen bond donor (D), hydrogen bond acceptor (A), and hydrophobic group (H). The pharmacophore models were generated by enabling the excluded volume shells for both actives and in-actives and number of features in a model were set to 4–7 features with deselecting the preferred number of minimum features in a pharmacophore model.

Validation of Pharmacophore model:

The generated pharmacophore model(s) were validated for effectiveness in identifying the active compounds using the Test set compounds and a decoy set. The test set consisted of 15 compounds out of which only 12 were deemed active according to the set criteria of the threshold pChEMbL value i.e. ≥7.2. The decoy set was generated by using DUD.E database [38]. The SMILES for active compounds (Test set) were used for the generation of decoys. A total of 1000 decoys were generated and were used along with the test set for the validation of pharmacophore model(s). Afterwards, the enrichment reports for each pharmacophore model were analyzed by using enrichment viewer wizard in PHASE.

Databases for Virtual Screening:

The databases used for virtual screening were FDA-approved DrugCentral structures (4088 structures) and, Enamine database (diversity set, 50,240 recently synthesized compounds)

a) DrugCentral (http://drugcentral.org) is a free and open online drug database. For FDA and other regulatory agency-approved active pharmaceutical compounds, DrugCentral integrates their structure, bioactivity, regulation, pharmacologic activities, and indications. Cross-referencing to external resources helps it complement other online resources. DrugCentral connects drug-target interactions to pharmacological action and indications at the molecular level. Text mining applications for data on drug adverse events and clinical trials are made possible by the integration with FDA drug labels. DrugCentral's FDA-approved medications and those found in four other chemical collections have similar chemical structures, as do five online drug sites [39].

b) A classical database of enumerated structures is the Enamine REAL database. The database is a resource for finding new hit molecules through extensive virtual screening and for looking for hit molecule analogs[40].

Compounds from each database were downloaded in 3D SDF format and each database is converted to PHASE database using LIGPREP [32] with EPIK [33] for the purpose of expanding the protonation and tautomeric states at physiological pH 7.0 ± 2 followed by the application of OPLS4 (optimized potential for liquid simulations) force field for the energy minimization using default parameters [34]. Additionally, conformers for each compound were created utilizing the create phase database wizard's conformer creation option. Virtual screening was performed for each database and afterwards, the top 3 HITs from each database were subjected to molecular docking studies.

Molecular Docking:

For the present study, sourcing from the Protein data bank, the X-ray crystal structure of human BACE-1 (PDB ID: 7MYI) was retrieved from Protein databank with a resolution of 1.25 Å [24]. The protein preparation wizard from Schrödinger interface [41] was used for the preparation of protein for docking analysis. The scaling factor was set to 1.0Å and the receptor grid was generated having the coordinates of 20.55 (x-axis), 55.6 (y-axis) and 87.68 (z-axis. For the purpose of molecular docking, Glide was utilized [42]. Moreover, the extra precision (XP) docking method was employed for molecular docking [43].

Molecular Mechanics-Generalized Born Surface Area (MM-GBSA) calculations:

In order to analyze the effect of solvent on the binding free energy of the molecules, the XP docked complexes were subjected to MM-GBSA utilizing PRIME from Schrödinger Suite [44]. To carry out the required calculations, two different force fields were applied namely, molecular mechanics and implicit solvation force fields [45].

The pose viewer files were used for the estimation of binding energies and PRIME local optimization tool was applied in order to minimize the docked poses. For the purpose of computing the binding free energies, the employed model consisted of VSGB solvent model [46], the OPLS4 force filed [47] and rotamer search algorithms [48] and is collectively called as the MM-GBSA continuum solvent model.

Molecular Dynamics Simulations:

The stability of the docked complex (BACE-1-Anileridine) was evaluated using MD simulation [49]. The ligand-protein complex which had the lowest MM-GBSA binding free energy was further submitted to DESMOND for MD simulations and the time frame was set to 50ns [50]. At first, a cubic simulation box was selected and furthermore, a TIP3P explicit water model constructed by using the system builder panel of DESMOND Schrodinger interface. The overall distance between the simulation box and the surface of protein was kept at 10Å. Moreover, in order to neutralize the system so there are no acidic and basic hindrances and to maintain the required isosmotic salt environment, a 150mM of sodium chloride was added. After 2000 iterations, the system was reduced to its most basic configuration. The minimized system was subjected to a 50 ns MD simulation utilizing the default relaxation option before simulation with the NPT ensemble at 300 K and 1.01 bars. The Nose-Hoover Chain thermostat[51] and Martyna-Tobias-Klein barostat [52] were used to sustain the said pressure and temperature, respectively. After every 10ps, energy and structure were measured and kept in the trajectory file. During the simulation, a time step of 2fs was taken into account. Trajectories and three-dimensional structures were examined using MAESTRO.

In-silico ADMET Profiling:

The *in-silico* ADMET profiling of the chosen drug molecule was done by using cloud version of ADMET Predictor (TM) version 10.4.0.5, 64-bit edition. All the parameters were calculated at the pH of 7.4.

Results

Training set phase database:

At first, a phase database was created for the training set compounds (36 inhibitors with known IC50 and pChEMbL values). Stereoisomers were produced by restricting or retaining some chirality's while allowing other chiral centers to change. Up to one low-energy conformation was created for rings with five to six members, and a maximum of four low-energy stereoisomers were preserved. Eighty-six compounds were ultimately obtained in all. Additionally, 4300 conformations in total were received, with an average of 50 conformations per molecule.

Description of the pharmacophore:

Using 36 recognized inhibitors of the BACE-1 enzyme, the common pharmacophore hypotheses were produced using the PHASE module of the Schrodinger Suite. Owing to the qualitative nature of the pharmacophore modeling process a characteristic framework was utilized which further helped in the development of model(s). In order to differentiate actives from in-actives a threshold pChEMbL value of 7.2 was used. By applying the threshold value all the compounds in training set with pChEMbL value of ≥ 7.2 were deemed active whereas compounds having pChEMbL value of less than 7.2 were deemed in-active. The pharmacophore hypotheses obtained are shown in **Table. 1**, while the corresponding IC_{50} values for each compound in the training set are shown in Fig. 4.

Out of 36 inhibitors, 27 inhibitors were deemed active according to the set criteria of the threshold value. The inactive compounds were 3, 5, 11, 12, 18, 19, 20, 21 and 27 having the IC_{50} values 100nM, 90nM, 120nM, 250nM, 150nM, 90nM, 130nM, 90nM and 630nM respectively. All the structures of training set molecules are shown in Fig. 6.

Table 1
shows the pharmacophore hypotheses identified by using PHASE module and their corresponding perfromance measuring metrices

Hypothesis	PhaseHypoScore	Survival Score	BEDROC Score	Site Score	Vector Score
AHRRR	1.328	6.253	0.953	0.807	0.961
HHRRR	1.237	6.275	0.861	0.760	0.923
AHHRRR	1.265	6.739	0.861	0.679	0.957

Based on the parameters mentioned in Table.1 for each of the obtained hypothesis, the hypothesis AHRRR was chosen as the best hypothesis among the bunch. Although the survival rate of the chosen

hypothesis is less than the other, the PhaseHypoScore (1.328) is the highest for the chosen hypothesis.

PhaseHypoScore provides a cumulative indication on the performance of the model [53]. The intra pharmacophoric feature distances and angles are shown in **Table.2** and **Table.3** respectively.

Table 2
Inter-feature site distance measurements of pharmacophore model AHRRR

Site 1	Site 2	Distance in A°	Site 1	Site 2	Distance in A°
A3	H7	2.99	H7	R12	7.68
H7	R11	5.85	H7	R10	5.85
A3	R11	4.09	A3	R12	7.28
A3	R10	4.09	R10	R12	8.67
R11	R12	4.27	R10	R11	4.71

Table 3
represents the inter-feature angle measurements of pharmacophore model AHRRR

Site 1	Reference	Site 2	Angle (°)	Site 1	Reference	Site 2	Angle (°)
H7	R12	A3	22.8	R12	H7	A3	71.0
R12	A3	H7	86.2	R11	A3	R10	70.3
A3	R10	R11	54.9	A3	R11	R10	54.9
A3	R11	R12	121.0	R12	A3	R11	30.2
A3	R12	R11	28.8	R12	R11	R10	149.6
R10	R12	R11	15.9	R11	R10	R12	14.4
H7	A3	R11	110.4	R11	H7	A3	41.0
A3	R11	H7	28.6	R10	A3	H7	110.3
R10	H7	A3	41.0	A3	R10	H7	28.6

A total of 5 features were identified in the chosen common pharmacophore hypothesis. The hypothesis contained one hydrogen bond acceptor, one hydrophobic, and three aromatic ring characteristics. After alignment of all the active ligands, it was revealed that all the active ligands possess all the 5

pharmacophoric features present in the hypothesis. The aligned active ligands with the hypothesis are shown in Fig. 5.

Pharmacophore modeling Validation:

A validation procedure is essential before implementing one or more pharmacophore models for use in real-world applications. Pharmacophore validation can be carried out by utilizing a variety of techniques, including the goodness of hit list (GH), the construction of receiver operating characteristic (ROC) curves, Fischer's method, or other statistical analysis, which depends on screening a test set and decoy set (if necessary) to assess the model's capacity to distinguish between active and inactive molecules and provide an estimation of its caliber [54]. Four factors primarily describe a model's quality: sensitivity (the ability to identify active compounds), specificity (the ability to rule out inactive molecules), yield of actives (the proportion of true positives to hits), and enrichment factor (which links yield of actives to the screening dataset's composition) [55]. Currently, a variety of metrics, including Area Under Receiver Operating Characteristic (AU-ROC), Relative Information Efficiency (RIE), Binary Ensemble Averaged ROC (BEDROC), and others, are utilized to assess how well ranking techniques function in virtual screening investigations[56–59]. The chemical structures of all the compounds of the test set are shown in Fig. 7.

A metric term BEDROC is used to assess the effectiveness of a virtual screening technique. The approach has a perfect score of 1.0 for each of the three evaluated alpha values, which demonstrates its strong enrichment power. ROC is a common statistic for assessing how well a binary classification system is working [60]. With an area under the curve (AUC) of 1.0, the outcome demonstrates that the approach has perfect performance. RIE gauges how well the method separates active molecules from decoys. A RIE of 17.70 indicates that the strategy is highly effective. The average number of outperforming decoys is zero, indicating that none of the active compounds outperformed by any of the decoys. All 12 active compounds are in the top N% of decoys for all tested percentages (1%, 2%, 5%, 10%, and 20%), according to the findings of the count and percentage of actives in top N% of decoys tests. All 12 active compounds are present in the top N% of results for all tested percentages (1%, 2%, 5%, 10%, and 20%), according to the count and percentage of actives in the top N% of results. The approach has a high enrichment power, as evidenced by the Enrichment Factors (EF) with respect to N% sample size and with respect to N% actives recovered. The approach can detect 80 times more active chemical compounds than would be predicted by chance, for example, the EF value for 1% sample size is 80.17. The percentage of the active set that is recovered by the approach is known as FOD (Fraction of Overall Discovery). The outcome demonstrates that the approach did not overlook any of the active chemicals.

Database Screening:

In order to identify the possible lead compounds against BACE-1 that could provide the treatment option for Alzheimer's disease, two databases were used for screening purpose. One of the databases was DrugCentral which contained FDA-approved drugs (4088) and the other one was Enamine diversity set database (50,240 compounds) which contains a large group of recently synthesized compounds which have not been tested yet. Both of the databases were first converted to Phase databases in order to

produce the possible conformers of the compounds. The procedure for the generation of Phase database was the same as mentioned earlier. The molecules were matched with at least 4 out of 5 pharmacophoric features of the pharmacophore hypothesis (AHRRR). Only top 3 hits from each database were chosen for further analysis. The top hits were chosen on the basis of PhaseScreenScore or FitnessScore that are mentioned in Table 4. Anileridine, Umifenovir and Doxapram were top 3 hits obtained as a result of screening of DrugCentral database and have been assigned codes A1, A2 and A3 respectively. Moreover, from enamine diversity set three molecules namely N-cyclopropyl-2-(4-(2-methylthiazol-4-yl)-1H-1,2,3-triazol-1-yl)-2-phenylacetamide, N-cyclopropyl-2-(4-(6-methylpyridin-2-yl)-1H-1,2,3-triazol-1-yl)-2-phenylacetamide and 5-(2-ethoxyphenyl)-3-(pyridin-4-yl)-1,2,4-oxadiazole and were assigned the codes B1, B2 and B3 respectively.

Anileridine was found to have the highest PhaseScreenScore of 2.077 and 5-(2-ethoxyphenyl)-3-(pyridin-4-yl)-1,2,4-oxadiazole having the lowest PhaseScreenScore of 1.951. These molecules were further subjected to further analysis to determine the inhibitory potential against human BACE-1 enzyme. The chemical structures of the Hit molecules are shown in Fig. 8 and the superimposed images of the Hit molecules with the pharmacophore hypothesis are shown in Fig. 9.

Table 4
represents top 3 hits from DrugCentral and Enamine diversity set along with their PhaseScreenScores for each hit molecule.

Database	Top 3 HITs	HIT Code	PhaseScreenScore
DrugCentral	Anileridine	A1	2.077
	Umifenovir	A2	2.042
	Doxapram	A3	2.004
Enamine Diversity Set	N-cyclopropyl-2-(4-(2-methylthiazol-4-yl)-1H-1,2,3-triazol-1-yl)-2-phenylacetamide	B1	1.983
	N-cyclopropyl-2-(4-(6-methylpyridin-2-yl)-1H-1,2,3-triazol-1-yl)-2-phenylacetamide	B2	1.981
	5-(2-ethoxyphenyl)-3-(pyridin-4-yl)-1,2,4-oxadiazole	B3	1.951

Molecular Docking using GLIDE:

The docking of both reference BACE-1 inhibitors and screened Hit molecules was done against human BACE-1 and the X-ray crystal structure of human BACE-1 (PDB ID: 7MYI) was downloaded from Protein data bank having a resolution of 1.25 A°[24]. The reference inhibitors 37, 44, 43, 47, 40, 50, 39, 51, 46 and 42 (taken from test set) were docked in the active site of the protein. Moreover, the co-crystallized ligand (compound 6) with 7MYI was also re-docked and evaluated for interactions. The important residues of the active site of the proteins have already been mentioned earlier and out of all those residues the most

important ones are Asp32 and Asp228 owing to the fact that they are involved in the normal catalytic process of the enzyme. The extra precision docking score and glide docking energies for all 10 reference inhibitors and screened hit molecules are all mentioned in Table 5.

Table 5
Docking and MM-GBSA results of reference inhibitors and Screened Hits against BACE-1

Docking and MM-GBSA results of reference inhibitors of BACE-1			
Ligands	XP Glide Score (Kcal/mol)	Glide Energy (Kcal/mol)	MM-GBSA dG Bind (Kcal/mol)
Compound 6 (Co-Crystallized ligand of 7MYI Re-docked)	-11.009	-85.105	-77.04
37	-9.077	-73.049	-65.03
44	-9.041	-63.094	-66.61
43	-9.038	-73.369	-60.42
47	-8.702	-68.335	-70.47
40	-8.553	-64.308	-67.60
50	-8.459	-65.987	-64.66
39	-8.371	-62.092	-63.65
51	-8.215	-65.734	-47.17
46	-6.071	-63.093	-17.71
42	-5.691	-75.213	-29.70
Docking and MM-GBSA results of screened Hits against BACE-1			
Anileridine (A1)	-6.914	-54.441	-49.14
Umifenovir (A2)	-6.144	-71.394	-39.14
Doxapram (A3)	-6.877	-49.927	-28.77
B1	-5.170	-62.102	-33.08
B2	-5.856	-60.838	-29.77
B3	-5.468	-42.641	-41.84

Interaction analysis of screened Hit compounds

The ligand interaction diagram (LID) of Schrodinger Suite was used to analyze the interaction pattern of reference inhibitors as well as screened hit compounds. The type of interaction, interacting atoms of

protein-ligand complex and interaction distances for reference inhibitors and screened hits are shown in Tables 6 and 7 respectively. All of the reference inhibitors showed interaction with the residues of the catalytic dyad i.e. Asp32 and Asp228 either by a hydrogen bond or a salt bridge. Figure 10 shows the interaction of compound 6 (co-crystallized ligand of 7MYI when re-docked).

Moreover, there were Pi-Pi stacking and Pi-Cation interaction present in most of the reference inhibitors which also help in providing strength to the ligand-protein complex and ultimately provide stability.

Table 6

shows Interaction analysis of referenced BACE-1 inhibitors against BACE-1

Sr. No	Ligands	Type of interaction	Interacting atoms of protein-ligand complex	Distances Å
1.	Compound 6	Hydrogen Bond	Asp228 …. Lig (N of NH_2)	2.17
		Hydrogen Bond	Asp32 …. Lig (N of NH_2)	1.83
		Hydrogen Bond	Asp32 …. Lig (N^+H of imidazole ring)	1.83
		Salt Bridge	Asp32 …. Lig (N^+H of imidazole ring)	2.85
		Pi-cation	Tyr71 …. Lig (N^+H of imidazole ring)	6.27
		Hydrogen bond	Trp76 …. Lig (N of pyrimidine ring via water bridge)	1.85 with H_2O molecule + 1.93 with ligand
7.	37	Hydrogen Bond	Asp228 …. Lig (N of NH_2)	2.29
		Hydrogen Bond	Asp32 …. Lig (N of NH_2)	1.81
		Hydrogen Bond	Asp32 …. Lig (N^+H of imidazole ring)	2.07
		Salt Bridge	Asp32 …. Lig (N^+H of imidazole ring)	2.96
		Pi-Cation	Tyr71 …. Lig (N^+H of imidazole ring)	6.41
12.	44	Hydrogen Bond	Asp228 …. Lig (N of NH_2)	2.02
		Hydrogen Bond	Asp32 …. Lig (N^+H of imidazole ring)	1.95
		Salt Bridge	Asp32 …. Lig (N^+H of imidazole ring)	2.96
15.	43	Hydrogen Bond	Asp228 …. Lig (N of NH_2)	2.14
		Hydrogen Bond	Asp32 …. Lig (N of NH_2)	2.21

Sr. No	Ligands	Type of interaction	Interacting atoms of protein-ligand complex	Distances Å
		Hydrogen Bond	Asp32 …. Lig (N$^+$H of imidazole ring)	2.06
		Salt Bridge	Asp32 …. Lig (N$^+$H of imidazole ring)	2.99
		Pi-Cation	Tyr71 …. Lig (N$^+$H of imidazole ring)	6.58
20.	47	Hydrogen Bond	Asp228 …. Lig (N of NH$_2$)	2.09
		Hydrogen Bond	Asp32 …. Lig (N of NH$_2$)	2.07
		Salt Bridge	Asp32 …. Lig (N$^+$H of imidazole ring)	2.97
		Pi-Cation	Tyr71 …. Lig (N$^+$H of imidazole ring)	6.59
24.	40	Hydrogen Bond	Asp228 …. Lig (N of NH$_2$)	2.01
		Hydrogen Bond	Asp32 …. Lig (N of NH$_2$)	2.04
		Hydrogen Bond	Asp32 …. Lig (N$^+$H of imidazole ring)	1.95
		Salt Bridge	Asp32 …. Lig (N$^+$H of imidazole ring)	2.96
28.	50	Hydrogen Bond	Asp228 …. Lig (N of NH$_2$)	2.00
		Hydrogen Bond	Asp32 …. Lig (N of NH$_2$)	2.04
		Hydrogen Bond	Asp32 …. Lig (N$^+$H of imidazole ring)	1.95
		Salt Bridge	Asp32 …. Lig (N$^+$H of imidazole ring)	2.96
32.	39	Hydrogen Bond	Asp228 …. Lig (N of NH$_2$)	2.10
		Hydrogen Bond	Asp32 …. Lig (N of NH$_2$)	2.11

Sr. No	Ligands	Type of interaction	Interacting atoms of protein-ligand complex	Distances Å
		Hydrogen Bond	Asp32 …. Lig (N$^+$H of imidazole ring)	1.97
		Salt Bridge	Asp32 …. Lig (N$^+$H of imidazole ring)	2.96
		Pi-Cation	Tyr71 …. Lig (N$^+$H of imidazole ring)	6.58
37.	**51**	Hydrogen Bond	Asp228 …. Lig (N of NH$_2$)	1.89
		Hydrogen Bond	Asp32 …. Lig (N of NH$_2$)	2.00
		Hydrogen Bond	Asp32 …. Lig (N$^+$H of imidazole ring)	2.07
		Salt Bridge	Asp32 …. Lig (N$^+$H of imidazole ring)	3.01
		Pi-Cation	Tyr71 …. Lig (N$^+$H of imidazole ring)	6.49
42.	**46**	Hydrogen Bond	Asp228 …. Lig (N of NH$_2$)	2.50
		Hydrogen Bond	Asp228 …. Lig (N of NH$_2$)	2.36
		Hydrogen Bond	Asp32 …. Lig (N of NH$_2$)	2.79
		Hydrogen Bond	Trp76 …. Lig (C)	1.91
46.	**42**	Hydrogen Bond	Asp228 …. Lig (N of NH$_2$)	2.28
		Hydrogen Bond	Asp32 …. Lig (N of NH$_2$)	1.92

However, in case of screened hit compound only Anileridine (A1) showed interaction with one of the residues of the catalytic dyad i.e. with Asp32 only. However, there were other amino acid residues which are involved in the binding interaction and the most prominent residues were Trp76 and Tyr71. The ligand atoms showed pi-pi stacking and pi-cation interaction and with a comparatively shorter distance when compared with reference inhibitors which could indicate a stronger binding with these residues. The most prominent docking score, docking energy score and ligand protein interactions were observed in Anileridine while B2 showed the least amount of residue and ligand interaction with only Trp76 involved

in making one hydrogen bond with the ligand molecule. The ligand interaction diagrams for all the screened hits are shown in Fig. 11. The involvement of Tyr71 and Trp76 in binding causes the conformation of BACE-1 enzyme to close which further contribute towards a stronger inhibition potential of the compounds[27].

The binding docking score and glide energy of B1 was the least prominent among the screened hits. The reference ligand 42 also showed the least significant score of -5.691kcal.mol and Anileridine showed a docking score of -6.914kcal.mol which is better when compared with ligand 42 and 46 both of which have shown inhibitory activity towards BACE-1 enzyme in in-vitro assays and possess a known IC_{50} values.

Table 7
shows Interaction analysis of screened Hit molecules against BACE-1

Sr. No	Ligands	Type of interaction	Interacting atoms if ligand-protein complex	Distances Å
1.	Anileridine (A1)	Salt Bridge	Asp32 …. Lig (N of piperidine ring)	4.82
		Pi-cation	Tyr71 …. Lig (N of piperidine ring)	4.87
		Hydrogen bond	Phe108 …. Lig (N of NH_2)	1.78
		Hydrogen bond	Lys107 …. Lig (N of NH_2)	2.09
5.	Umifenovir (A2)	Hydrogen bond	Trp76 …. Lig (O)	2.34
		Hydrogen bond	Gly34 …. Lig (O)	2.16
		Pi-Pi Stacking	Tyr71 ….Lig (Pyrole ring)	4.23
		Hydrogen bond	Tyr198 …. Lig (O)	2.10
9.	Doxapram (A3)	Hydrogen Bond	Gly230 …. Lig (N of piperidine ring)	1.90
		Pi-Pi Stacking	Tyr71 …. Lig (benzene ring)	4.48
11.	B1	Hydrogen Bond	Trp76 …. Lig (triazole ring)	2.69
12.	B2	Hydrogen bond	Trp76 …. Lig (N of triazole ring)	2.41
		Pi-Pi Stacking	Tyr71 …. Lig (triazole ring)	3.96
14.	B3	Hydrogen bond	Trp76 …. Lig (O)	1.97
		Pi-Pi Stacking	Tyr71 …. Lig (benzene ring)	4.35

Molecular Mechanics - General Born Surface Area (MM-GBSA) Analysis:

The MM-GBSA values for referenced inhibitors and the screened hits are shown in Table 5. The range of MM-GBSA for referenced inhibitors was between – 17.71kcal/mol and – 70.47kcal/mol. Out of all the screened hits anileridine (A1) had the binding free energy of -49.14kcal/mol which was considered the best among the screened hits. Obtained results suggest the formation of a stable ligand-protein complex between anileridine and BACE-1. Hereby, in view of this argument we selected anileridine for further analysis and was subjected to molecular dynamic simulation and *in-silico* ADMET profiling.

Molecular Dynamic Simulations analysis:

MD simulation is used to analyzed and assess the stability and dynamics profile of the docked protein-ligand complex. For a simulation time of 50ns, the docked complex of anileridine-BACE-1 was subjected to MD simulation. According to Fig. 12, The fact that the Root mean square deviations (RMSD) followed somewhat comparable tracks during the latter part of the first half (15-30ns) and early second half (30-45ns) of the simulation indicates that the entire system was well equilibrated. In contrast, the complex form's trajectory completely converged with the Apo form (no ligand) between 35ns and 40ns. Moreover, the trajectory of the complex for also converged to some extent with the Apo form 15ns to 25ns during the simulation. The RMSD for the complex and Apo forms, respectively, ranged from 0.25 to 1.0Å and 1.0 to 1.75Å during the first half of the simulation. The RMSD maintained substantially below 0.1 throughout the second half of the simulation. While the RMSD of the complex fluctuated between 0.25 and 2.0Å, that of the Apo form fluctuated between 1.75 and 2.0Å. From 35ns-40ns the complex converged with the Apo form completely and from 15ns-25ns the complex converged with the Apo form slightly to some extent. Altogether, these results showed a stable binding interaction between anileridine and BACE-1 protein upon formation of substantial interactions with key amino acids of the binding pocket.

The ligand-protein interactions were monitored throughout the time of the simulation. Protein ligand interactions were categorized into 4 major types namely: hydrogen bonds, ionic interactions, water bridges and hydrophobic interactions and are shown in Figs. 13 and 14. Throughout the trajectory, the stacked bar charts (Fig. 11) were normalized, for example a value of 0.8 is an indication that for 80% of the simulation time the specific interactions were maintained. In accordance with the stacked bar charts, the interaction fraction of ligand with Asp32 is approximately 0.8 and accompanied by 3 types of interactions. For an interaction fraction of 0.15 there were hydrogen bonds afterwards from 0.15–0.78 there were ionic interactions and finally for a very brief period of time there were water bridges. The interaction fraction of ligand with Tyr71 was well above 1.2 whereas the interaction fraction with Asp228 was around 0.2 with only ionic interaction and water bridges. The interaction fraction with Phe108 was found to be 0.7 with mostly hydrophobic interaction. Finally, the interaction fraction with Gly74 was approximately 0.6 with only hydrogen bonding as the interaction force. Other amino acids in the stacked bar charts showed minor interactions for a very short period of time.

For ligand binding to occur, hydrogen bonds are crucial. Because they have such a significant impact on drug specificity, metabolism, and adsorption, hydrogen-bonding qualities should be taken into account while developing novel drugs. Four further subtypes of hydrogen bonds can be distinguished between a protein and its ligand: backbone acceptor, backbone donor, side-chain acceptor, and side-chain donor [53].

Figure 15 shows the total time of simulation on x-axis and amino acid interaction with the ligand on y-axis. The figure shown the time of interaction of each amino acid involved throughout the time of simulation (50ns). According to this, Asp32 shows the one of the strongest interaction with the ligand. Asp32 showed continuous interaction with only minor break throughout the simulation making the interaction stable. On the other hand, Asp228, another important amino acid of the catalytic dyad as mentioned before showed interaction but for only about 12-13ns which was not shown during molecular docking. Other important and strong, continuous interactions were shown by Tyr71, Phe108 and Gly74. Gly74 started showing interaction in the late part of the first half of simulation but the interaction remained strong afterwards till the end of simulation with only minor breaks. Tyr71 showed interaction even stronger and with less breaking point than Asp32 and as mentioned before interaction of ligand with Tyr71 caused the conformation of protein to close making the inhibition even stronger. Similarly, Phe108 showed significant strong interaction with minor breaks throughout the simulation time. Moreover, Arg235 did not show any interaction in molecular docking but in MD simulations since the environment is dynamic and it also has water molecules Arg235 forms a water bridge and then a contact with the ligand atom which is also evident in Fig. 14 as well.

Figure 16 shows the torsional profile of Anileridine obtained via MD simulations. There are a total of 8 rotatable bonds in anileridine and are color coded with different colors. There are two types of plots in this figure, the bar plot and the radial plot and explain the probability density of the torsion and conformation of torsion respectively throughout the course of simulation (0-50ns). The bar and dial plots of the rotatable bond between benzene ring and piperidine ring (colored in blue) show that this bond is rotating on both x-axis and y-axis with a significant degree of freedom (almost a complete 180° rotation in both positive and negative x-axis. However, the bar and dial plots of a bond between amine and benzene ring (colored in dark orange) show that the rotation of bond is predominantly towards 90° of the positive x-axis.

Moreover, the rotatable bond between nitrogen of piperidine and -CH_2 (colored in purple) shows a rotation of 90° towards negative x-axis. Similarly, the rotatable bond between the carbonyl carbon and oxygen atom (colored in pink) shows a specific rotation of 180° in both positive and negative x-axis. On a similar note, other rotatable bonds are also color coded and are their torsional profile is shown in both dial (radial) and bar plots.

ADMET Profile: Anileridine

Predictive Absorption, Distribution, Metabolism, Excretion and Toxicity (ADMET) studies are the largest area of interest in drug discovery and development. Utilizing enormous databases of ADMET data associated with structures, the objective is to create computer models that link structural changes with changes in response. These models can be used to create and predict molecules with superior properties. Additionally, these databases enable users to estimate human ADMET features by extrapolating human in vitro and animal in vivo ADMET results [61]. In order to aid researchers in creating efficient dosage forms for currently existing molecules, these databases or software also offer helpful information on

those molecules. For this investigation, numerous parameters concerning Anileridine (PubChem ID: 8944) were predicted using the cloud version of ADMET Predictor (TM) version 10.4.0.5, 64-bit edition.

1. Predictive Physicochemical (Absorption and Distribution) Profile:

Physicochemical properties of drug molecules play an important role in transforming a new molecular entity into a suitable dosage form. It is necessary for a drug molecule to exert its optimal activity to have good solubility, permeability, dissolution rate and pre-systemic metabolism [62]. Since then, while extensive evaluations have investigated the relationship with metabolic stability and toxicity, physicochemical properties of a molecule that are consistent with the likelihood of good oral absorption have been further developed. Thorough analyses of the physicochemical aspects of drug-target interactions have supported these conclusions. The distinctive characteristic of best-in-class pharmaceuticals, according to thermodynamic profiling, is a reliance on enthalpy, which depends on lipophilicity, to drive binding energetics [63].

The predictive ADMET profile was calculated at 7.4 pH value. The values for MLogP and Volume of distribution (V_d) indicate that the drug is hydrophobic in nature and the blood brain barrier (BBB) filter value is 99% which is an indication of drug's ability to cross BBB. In case of Alzheimer's disease it is imperative for the drug molecule to cross the BBB and Anileridine possesses the ability to a significant level of confidence. MLogP is one of the simplest methods developed by Moriguchi for estimating the LogP value of the drug molecules by taking structural features of the drug into consideration [64]. The BCS class of anileridine is shown in Fig. 17.

The detailed physicochemical profile of Anileridine is given in Table 8.

Table 8

shows the important physicochemical parameters and their predicted values by the model.

Sr.#	Parameter	Predictive value	Model used and explanation
1.	MlogP	2.96	Moriguchi estimation of log P [64].
2.	Permeation Cornea	180.523	Permeability through the rabbit cornea (cm/s x 10^7).
3.	S + logP	3.467	Simulations Plus model of log P.
4.	S + Acidic_pKa	None	Macroscopic predictions of the pKa values appear to be governed by the predominant acidic groups
5.	S + Basic_pKa	8.47; 4.25	Macroscopic predictions of the pKa values appear to be governed by the predominant basic groups
6.	Solution Factor	224.578	Universal salt solubility factor based on S + Sw model.
7.	Vd	3.477	Volume of distribution (L/kg) in human at steady state.
8.	Water Solubility (S + Sw)	0.15	Water solubility in mg/mL of the given compound predicted by the model on the basis of chemical features
9.	Diffusion coefficient	0.646	Water diffusion coefficient of nonelectrolytes at infinite dilution by Hayduk-Laudie (cm2/s x 105).
10.	S + MDCK-LE permeability assay	High (99%)	MDCK permeability classification model (low or high) built on Varma et al. data for ECCS.
11.	S + logD	2.367	log D, at 7.4 pH, based on S + logP.
12.	BBB Filter	Yes (99%), High	Determines whether a substance will be able to cross the blood−brain barrier.
13.	Permeation Skin	5.056	Permeability through human skin (cm/s x 10^7).
14.	Simulated metabolic clearance (S + CL_Metabolism)	Yes (99%)	Predicts whether clearance mechanism is metabolic.
15.	Simulated Renal Clearance (S + CL_Renal)	No (99%)	Predicts whether clearance mechanism is renal.
16.	Simulated human jejunal permeability (S + Peff)	2.161	Effective human jejunal permeability (cm/s x 10^4).
17.	hum_fup%	13.642	Percent UNBOUND to blood plasma proteins in human.

Sr.#	Parameter	Predictive value	Model used and explanation
18.	ECCS_Class	Class 2	Major clearing mechanisms of drug and drug like molecules that are described in the ECCS class. based on the article of Varma et al. 1A = metabolism, 1B = hepatic uptake, 2 = metabolism, 3A = renal, 3B = either renal or hepatic uptake, and 4 = renal [65]

The model showed that the drug has a significant clearance via metabolic pathway and almost no renal clearance in unchanged form. Moreover, the drug has an acceptable jejunal permeability profile along with very good cornea permeation and skin permeation profile. According to the model the drug belongs to Class 2 of Extended Clearance Classification System (ECCS) which indicates that the major route of clearance of Anileridine is via metabolic route.

1.1. Solubility profile in relation to pH:

Several factors such as drug solubility, permeability, first pass metabolism and dissolution rate etc. may influence the ultimate oral absorption of the drug molecules and out of these parameters usually the poor solubility of the drug is contributed to poor oral absorption [66]. The model predicted the solubility of the drug and is shown in Fig. 18. It depicts that the drug has a good solubility profile at acidic pH and has a maximum peak level at pH value of 4.5. However, by increasing the pH value towards neutral conditions the solubility of the drug decreases many folds. Moreover, at basic pH the solubility is almost near to zero.

1.2. pKa Microstates:

The pka macro-state values display the drug's maximal concentration at a given pKa value. The concentration of hydrogen ions (pH) at which 50% of the drug resides in its ionized hydrophilic form is known as the drug's pKa (i.e., the pH at which it is in balance with its unionized lipophilic form). All local anesthetics are known to have a basic moiety in their structures and are considered to be weak bases. At physiological pH, the pKa value decreases as the lipophilicity rises [67]. The value of pKa represents the acidity and basicity of a balanced aqueous solution. For the drug to absorb, the compounds inside must be electrically neutral; otherwise, the medicinal product will not be permeable enough.

According to the model the drug possesses 0 acidic atom(s) and 2 basic atom(s): 4(-NH2)3(>N-). The model was built by only micro species contributing more than 1.0% are displayed. Moreover, Aliphatic -OH and amides groups were ignored as well as carbon protonation. The drug is 100% at a pKa values of 8.47 and 4.25 either in protonated form or in neutral form. The relationship of pKa with the microstates and macro-states of the drug is shown in Fig. 19.

1.3. Log D profile:

While conducting studies to determine the LogD profile of drug molecules it is necessary to monitor and control the pH and ionic strength especially while working with ionizable compounds [68]. The predictive

LogD profile of anileridine in relation to pH suggest that at low pH the drug has almost zero diffusion rate however, as the pH starts to increase the drug will start to diffuse and by the time pH reaches 10, the diffusion rate of the drug will become optimal. The data gives the indication that by controlling and manipulating the pH the higher degree diffusion of anileridine can be achieved. The relationship of increasing pH on diffusion coefficient of anileridine is shown in Fig. 20.

2. Predictive metabolic profile:

Drug metabolism investigations are crucial for a number of reasons, including the discovery of novel chemical entities based on the identification of active metabolites, limiting potential safety risks brought on by the production of reactive or toxic metabolites, ensuring potential adequate coverage of human metabolites in animals, assisting in the prediction of human doses, and comparing preclinical metabolism in animals with that of humans [69].

From CYP450 class of metabolic enzymes only CYP2C8, CYP3A4 and CYP2D6 were found to be involved in the metabolism of anileridine. The sites of metabolism of each enzyme on the drug are shown in Fig. 21.

CYP3A4 was found to be the most prominent of the bunch to be involved in metabolism of the drug molecule. The structures of predictive metabolites and percentage of each metabolite formation is shown in Fig. 20A. Besides CYP450, UDP-glucuronosyltransferase (UGT) is also involved to some extent in the metabolism of the drug molecule. UGT1A1, UGT1A4, UGT2B7 and UGT1A3 were mostly metabolizing the drug. The chemical structures of the predictive metabolites are shown in Fig. 20B. The model predicted two major metabolites, one having sugar attached to the free amino group and the second one having sugar attached to the nitrogen of the piperidine ring. According to the predicted model UGT1A1, UGT1A4, UGT2B7 were mostly producing the metabolite 1 (M1) while UGT1A3 was predominantly making the metabolite 2 (M2). The numerical values for different parameters of enzyme metabolism are given in **Table 22.**

Table 9
shows important parameters of enzyme metabolism and their predicted numerical values

Sr. #	Parameter	Predictive value	Model used and explanation
1.	CYP3A4_Clint	28.799	According to the model, it shows the predicted CYP3A4 mediated oxidation (uL/min/mg HLM protein) which also represents the pooled atom level intrinsic clearance for the said protein.
2.	CYP3A4_HLM_Clint	91.149	According to the model, it shows the predicted CYP3A4 mediated oxidation (uL/min/mg HLM protein) in human hepatic microsomes and also represents the pooled atom level intrinsic clearance for the said protein
3.	CYP3A4_HLM_Km	22.581	Km represents the Michaelis-Menten constant for the oxidation reaction in human hepatic microsomes in unbound form and is mediated by CYP3A4 at atom level. The unit of measure a µM.
4.	CYP3A4_HLM_Vmax	2.058	Vmax is the Michaelis-Menten constant (nmol/min/mg HLM Protein) corresponding to the oxidation reaction in human hepatic microsomes. The reaction is mediated by CYP3A4.
5.	Hepatic clearance (HEP_hCLint)	46.234	Intrinsic clearance in uL/min/million cells for metabolism in human hepatocytes (unbound form).
6.	HEP_mCLint	22.448	Intrinsic clearance in uL/min/million cells for metabolism in mouse hepatocytes (unbound form).
7.	HEP_rCLint	486.67	Intrinsic clearance in uL/min/million cells for metabolism in rat hepatocytes (unbound form).
8.	CYP2D6_Vmax	1.736	Vmax is the Michaelis-Menten constant (nmol/min/mg HLM Protein) corresponding to the oxidation reaction in human hepatic microsomes. The reaction is mediated by CYP2D6.

Predictive transport profile:

Nowadays, it is generally accepted that drug transporters play a significant role in determining how well drugs are absorbed, excreted, and, in many circumstances, how extensively they penetrate target organs. Additionally, there is a growing understanding of how changed drug transporter function, whether brought on by genetic polymorphisms, drug-drug interactions, or environmental elements like dietary components, may cause unanticipated toxicity [70].

According to the predicted model, anileridine was found to be a substrate of p-glycoprotein (63%) as well as an inhibitor of both types Organic Cation Transporter (OCT) 1 and 2. OCT 1 and OCT 2 are transport proteins that are involved in the transport of cations across the membranes of liver and kidney respectively hence if a drug is to inhibit these transport proteins then ultimately their metabolism and renal excretion would be compromised and the drug might cause toxicity. In these instances, if the drug is

a known inhibitor of any of these two transport proteins then it is suggested to decrease the dose of the drug to counter the toxicity.

3. Predictive toxicity profile:

Instead of just determining how safe a medicinal entity is, the aim of toxicity testing is to uncover any potential dangerous effects that it may have. Finding out how drug compounds behave in lab animals and whether they have any potentially harmful effects on humans directly are the main objectives of toxicity testing. Additionally, they involve administering huge doses to lab animals in order to determine any potential dangers to humans who are exposed to much lower amounts [71]. Additionally, there are currently a number of in silico tools that can estimate the prospective toxicity potential of drug molecules as well as the expected toxicity profiles of previously discovered drugs. These tools may ultimately aid researchers in developing effective dosage forms and delivery systems for the already existing drugs in order to reduce their toxic effects. The important parameters are mentioned in Table 10.

Table 10
represents the important toxicity parameters of anileridine and their predicted values

Sr. #	Parameter	Predictive value	Model used and Explanation
1.	Bio-concentration factor	10.375	In steady state, the bio-concentration factor (also known as the concentration ratio [Cfish/Cwater]) is a partition coefficient between fish tissues and environmental water.
2.	Chromosomal Aberration	Nontoxic (88%)	Determines if the substance will cause the mutagenic chromosomal abnormalities.
3.	hERG Filter	Yes (75%)	Determines if the substance will block the hERG potassium channel and has the potential for cardiotoxicity
4.	hERG_pIC$_{50}$	5.503	Human pIC_50 (mol/L) expression of affinity to the hERG potassium channel.
5.	Reproductive toxicity	Nontoxic (96%)	Qualitative assessment of developmental and reproductive toxicity.
6.	Serum ALT	Normal (81%)	Determines whether or not a molecular entity will result in a rise in SGPT enzyme levels.
7.	Serum ALP	Normal (92%)	Determines whether or not the molecular entity will raise the levels of the enzyme alkaline phosphatase.
8.	Serum AST	Elevated (76%)	Determines whether or not the molecular entity will raise the levels of the Human SGOT enzyme.
9.	Serum GGT	Normal (80%)	Determines if a molecular entity will raise the levels of the GGT enzyme.
10.	Serum LDH	Normal (94%)	Determines if a molecular entity will result in an increase in LDH enzyme levels.
11.	Rat_TD50	10.927	TD50 (mg/kg/day in oral dose) for rat carcinogenicity over a typical lifetime.
12.	PLipidosis	Toxic (82%)	Qualitative estimation of causing phospholipidosis.
13.	Estro_Filter	Toxic (79%)	Predicts whether or not the compound possesses estrogen receptor toxicity in rat.
14.	Andro_Filter	Toxic (68%)	Predicts whether or not the compound possesses androgen receptor toxicity in rat.

The predictive toxicity profile revealed that the drug is cardio-toxic as the hERG filter value is 75% and hERG pIC$_{50}$ is 5.503 which is significantly high. Moreover, the drug shows toxicity towards bot androgen and estrogen receptors in rat. However, the drug is not hepatotoxic as it only mildly elevates serum AST levels. The drug is non-mutagenic and non-toxic to chromosomal proteins (histone) as well as shows no reproductive toxicity.

4. Simulated Pharmacokinetic profile:

For a therapeutic molecule to be properly transformed into a formulation that would ultimately deliver the best efficacy with the fewest adverse effects, pharmacokinetic characteristics are crucial. Today, a variety of *in-silico* methods are utilized to calculate pharmacokinetic parameters including volume of distribution, AUC, Cmax, and Cmin [72].

Using the cloud version of ADMET Predictor (TM) version 10.4.0.5, 64-bit, a Cp vs. Time curve was plotted. The modelled pharmacokinetic characteristics were predicted using an initial dose of 10mg/kg administered intravenously and per oral. The simulated PK and biopharmaceutical profile is shown in **Figure 23**.

The bioavailability of the given drug was virtually 100% in the first scenario since it was administered intravenously. 7.59ng/ml and 44.96ng/ml, respectively, were the C_{min} and C_{max} predicted values. Additionally, AUC_{inf} was 601.85ng-h/ml and the area under the curve (AUC) was roughly 498.58ng-h/ml. According to the Cp vs. time curve, the estimated half-life $(t_{1/2})$ was 9.28 hours, and the apparent volume of distribution (V_d) was 222.41 L. Anileridine has a clearance (Cl) value of 16.61 L/h and a Cl_p value of 16.61 L/h.

Oral IR tablets, on the other hand, had C_{min} and C_{max} predicted values of 6.61ng/ml and 29.58ng/ml, respectively. Additionally, the area under the curve (AUC) was around 392.16ng-h/ml, and the AUC_{inf} value was 482.14ng-h/ml. The apparent volume of distribution (V_d) was 222.41 L, and the estimated half-life (t1/2) from the Cp vs. time curve was 9.28 hours. Anileridine's clearance (Cl) and Cl_p values are both 16.61 L/h. The T_{max} for anileridine when taken orally was reported to be 2.57 hours.

Discussion

Alzheimer's disease is an aging brain ailment that causes neuronal degradation [73]. The steady deterioration in cognitive function of those who have Alzheimer's disease (AD) makes it one of the most financially draining diseases in the world. Small, imperceptible brain changes that precede the onset of AD's symptoms are thought to start long before the symptoms themselves. AD is a chronic degenerative illness since it worsens with time [2].

Several hypotheses are linked with the pathophysiology of AD. Out of these, the amyloid hypothesis is one of the most important. The amyloid hypothesis suggests that neurodegeneration is caused by the deposition of amyloid-β (Aβ) peptides in the brain. β-secretase and γ-secretase cleaves amyloid precursor protein (APP) leading to the formation of Aβ fragments [74]. Since amyloid deposition is one of the hallmark features observed in AD patients and due to the direct involvement of BACE-1 in the aggregation of these plaques, strategies to inhibit the action of the aforementioned enzyme would be able to stop the aggregation of the said plaques and subsequent arrest of disease in early stages.

Since the characterization of BACE-1 more than 2 decades ago [75], the inhibition of the protein has been considered as the most important strategy to assess the amyloid hypothesis. However, search for novel compounds is time taking and expensive. In view of this a strategy called drug repurposing is a promising alternative. Drug repurposing or repositioning is a strategy that refers to the application of a drug molecule approved by the regulatory agencies for an otherwise off-label disease [76]. One of the major advantages of drug repurposing is the availability of large volumes of data regarding clinical tests, toxicity profile, chemical composition, and synthesis methodologies which would ultimately accelerate the process of their application in clinical trials [77]. In order to save time and accelerate the process of discovery of compounds against several ailments via drug repurposing strategy, ligand based pharmacophore modeling and *in-silico* studies propose a very promising avenue. Several studies have been published in which pharmacophore modeling has proven successful. In a study a group of researchers reported the discovery of potential topoisomerase I inhibitors via ligand based pharmacophore modeling and virtual screening [78]. Other studies have also reported corticotropin releasing factor receptor antagonists [79], potent isoprenylcysteine carboxyl methyltransferase (Icmt) inhibitors [80], identification of lead compounds for Chk1[81], N-methyl pyrimidones as HIV-1integrase inhibitors [82], non-steroidal aromatase inhibitors [83], breast cancer migration and proliferation inhibitors [84], potential lumazine synthase inhibitors [85] and new MurF inhibitors [86].

In the present study, a pharmacophore model (AHRRR) was established for the identification of significant pharmacophore features of BACE-I inhibitors gathered from the literature search and ChEMbL database. The established pharmacophore model AHRRR was within the upper limit of the acceptable range with EF1% of 80.17 and there were no decoys out ranking the active compounds. Top Hits included anileridine, Umifenovir and Doxapram from FDA-approved database and 3 hits were obtained from enamine diversity set. Molecular docking (-6.914kcal/mol) and MM-GBSA (-49.14kcal/mol) analysis revealed anileridine as the best compound to be further subjected to molecular dynamic simulation and *in-silico* ADMET profiling. Molecular docking as revealed in previous study can successfully predict the binding modalities of small molecules (ligands) with the binding pocket of the receptor protein [87]. The MD simulation of anileridine showed the formation of stable ligand-protein complex in dynamic conditions and also making strong contacts with one of the two important aspartic acid residues i.e. Asp32. For facilitating the process of lead compound discovery and optimization, MD simulations provide an in-depth analysis of binding energies and molecular kinetics of protein-ligand complex, therefore provide a clear understanding for choosing the best drug molecule for further development [88]. MD simulations can also expedite the process of drug discovery by identification of allosteric sites of a protein molecules as well as precise prediction of binding free energy of drug candidates thereby improving the traditional virtual screening approaches [89]. The ADMET profiling depicted that anileridine possesses a high affinity for crossing BBB which is a pre-requisite for drug acting on central nervous system (CNS). Furthermore, anileridine was found to be non-toxic towards liver, reproductive system, chromosomes and bile salt protein but was found to have toxic potential for CVS system, androgen and estrogen receptors. Lead molecule development now offers a new perspective thanks to early-stage ADMET analysis. Despite the availability of a number of high-throughput in vitro models for ADMET

profiling, in silico approaches are becoming more and more popular due to their ability to predict outcomes quickly and affordably without the use of time-consuming or expensive laboratory facilities[90].

Finally, our study suggests that anileridine has the potential to inhibit BACE-1 enzyme and can be further tested both in-vitro and in-vivo. Moreover, the hits obtained in this study can serve as lead compounds for designing and optimizing BACE-1 inhibitors.

Conclusion

The study reported the successful generation and validation of a pharmacophore model with subsequent virtual screening. Virtual screening of FDA-approved DrugCentral database and Enamine diversity set (Enamine database) produced 3 hits each which were further subjected to molecular docking, MM-GBSA analysis which resulted in identification of anileridine as the potential BACE-1 inhibitor. Anileridine showed significant interaction with one of the important amino acids of the catalytic dyad of BACE-1 enzyme i.e. Asp32. Furthermore, MD simulations supported the molecular docking and MM-GBSA results and revealed the formation of stable interaction between anileridine and BACE-1. After establishing anileridine as the potential BACE-1 inhibitor procured from already approved drugs, it was subjected to extensive in-silico studies using the cloud version of ADMET Predictor (TM) version 10.4.0.5, 64-bit edition. The analysis showed that the drug is permeable to BBB, non-toxic to hepatocytes, reproductive system, kidneys, and chromosomal proteins and is also non-mutagenic. However, the drug was found to be cardio-toxic, toxic to androgen and estrogen receptors. Furthermore, the drug was found to be a substrate of p-glycoprotein and belongs to BCS class 1 and ECCS class 2. The obtained results also suggested that this model (AHRRR) can be used to rationally design novel inhibitors of BACE-1 and also identify new molecules from databases as BACE-1 inhibitors.

Declarations

Ethical approval and consent for participation:

Not applicable

Consent for publication:

The authors give consent for the publication

Availability of data and material

Not applicable

Competing interest:

There are no competing interests of any author to declare

References

1. Kumar, A., et al., *Alzheimer Disease*, in *StatPearls*. 2023, StatPearls Publishing Copyright © 2023, StatPearls Publishing LLC.: Treasure Island (FL) ineligible companies. Disclosure: Jaskirat Sidhu declares no relevant financial relationships with ineligible companies. Disclosure: Amandeep Goyal declares no relevant financial relationships with ineligible companies. Disclosure: Jack Tsao declares no relevant financial relationships with ineligible companies.

2. Association, A.s., *2019 Alzheimer's disease facts and figures.* Alzheimer's & dementia, 2019. **15**(3): p. 321-387.

3. De-Paula, V.J., et al., *Alzheimer's disease.* Subcell Biochem, 2012. **65**: p. 329-52.

4. Reiman, E.M., et al., *Brain imaging and fluid biomarker analysis in young adults at genetic risk for autosomal dominant Alzheimer's disease in the presenilin 1 E280A kindred: a case-control study.* The Lancet Neurology, 2012. **11**(12): p. 1048-1056.

5. Koelsch, G., *BACE1 Function and Inhibition: Implications of Intervention in the Amyloid Pathway of Alzheimer's Disease Pathology.* Molecules, 2017. **22**(10).

6. Wong, W., *Economic burden of Alzheimer disease and managed care considerations.* Am J Manag Care, 2020. **26**(8 Suppl): p. S177-s183.

7. Skaria, A.P., *The economic and societal burden of Alzheimer disease: managed care considerations.* Am J Manag Care, 2022. **28**(10 Suppl): p. S188-s196.

8. Nandi, A., et al., *Global and regional projections of the economic burden of Alzheimer's disease and related dementias from 2019 to 2050: A value of statistical life approach.* eClinicalMedicine, 2022. **51**.

9. Adamson, M.M., et al., *Brain injury and dementia in Pakistan: current perspectives.* Frontiers in neurology, 2020. **11**: p. 299.

10. Pushpakom, S., et al., *Drug repurposing: progress, challenges and recommendations.* Nature Reviews Drug Discovery, 2019. **18**(1): p. 41-58.

11. Breckenridge, A. and R. Jacob, *Overcoming the legal and regulatory barriers to drug repurposing.* Nature Reviews Drug Discovery, 2019. **18**(1): p. 1-2.

12. Roy, K., S. Kar, and R.N. Das, *Chapter 10 - Other Related Techniques*, in *Understanding the Basics of QSAR for Applications in Pharmaceutical Sciences and Risk Assessment*, K. Roy, S. Kar, and R.N. Das, Editors. 2015, Academic Press: Boston. p. 357-425.

13. Tyagi, R., et al., *Chapter 17 - Pharmacophore modeling and its applications*, in *Bioinformatics*, D.B. Singh and R.K. Pathak, Editors. 2022, Academic Press. p. 269-289.

14. Shoichet, B.K., *Virtual screening of chemical libraries.* Nature, 2004. **432**(7019): p. 862-5.

15. Opo, F.A.D.M., et al., *Structure based pharmacophore modeling, virtual screening, molecular docking and ADMET approaches for identification of natural anti-cancer agents targeting XIAP protein.* Scientific Reports, 2021. **11**(1): p. 4049.

16. Maia, E.H.B., et al., *Structure-Based Virtual Screening: From Classical to Artificial Intelligence.* 2020. **8**.

17. Kaserer, T., et al., *Pharmacophore Models and Pharmacophore-Based Virtual Screening: Concepts and Applications Exemplified on Hydroxysteroid Dehydrogenases.* Molecules, 2015. **20**(12): p. 22799-832.

18. Yen, Y.C., et al., *Development of an Efficient Enzyme Production and Structure-Based Discovery Platform for BACE1 Inhibitors.* 2019. **58**(44): p. 4424-4435.

19. Taylor, H.A., et al., *BACE1: More than just a β-secretase.* Obesity Reviews, 2022. **23**(7): p. e13430.

20. Mouchlis, V.D., et al., *Computer-Aided Drug Design of β-Secretase, γ-Secretase and Anti-Tau Inhibitors for the Discovery of Novel Alzheimer's Therapeutics.* Int J Mol Sci, 2020. **21**(3).

21. Hernández-Rodríguez, M., et al., *Asp32 and Asp228 determine the selective inhibition of BACE1 as shown by docking and molecular dynamics simulations.* European Journal of Medicinal Chemistry, 2016. **124**: p. 1142-1154.

22. Munj, S.M. and P.B. Patil, *Drug Discovery to Drug Development of BACE1 Inhibitor as Antialzheimer's: A Review.* Current Topics in Medicinal Chemistry, 2023. **23**(2): p. 77-97.

23. Kocak, A., et al., *Computational insights into the protonation states of catalytic dyad in BACE1−acyl guanidine based inhibitor complex.* Journal of Molecular Graphics and Modelling, 2016. **70**: p. 226-235.

24. Rose, P.W., et al., *The RCSB Protein Data Bank: new resources for research and education.* Nucleic acids research, 2012. **41**(D1): p. D475-D482.

25. Rombouts, F.J.R., et al., *Fragment Binding to β-Secretase 1 without Catalytic Aspartate Interactions Identified via Orthogonal Screening Approaches.* ACS Omega, 2017. **2**(2): p. 685-697.

26. Moussa-Pacha, N.M., S.M. Abdin, and H.A. Omar, *BACE1 inhibitors: Current status and future directions in treating Alzheimer's disease.* 2020. **40**(1): p. 339-384.

27. Yuan, J., et al., *Structure-based design of β-site APP cleaving enzyme 1 (BACE1) inhibitors for the treatment of Alzheimer's disease.* J Med Chem, 2013. **56**(11): p. 4156-80.

28. Gaulton, A., et al., *ChEMBL: a large-scale bioactivity database for drug discovery.* Nucleic acids research, 2012. **40**(D1): p. D1100-D1107.

29. Schrödinger, M., *Schrödinger Release 2023-3: Maestro, Schrödinger, LLC, New York, NY, 2023.* 2023.

30. Wetzel, S., et al., *Interactive exploration of chemical space with Scaffold Hunter.* Nature chemical biology, 2009. **5**(8): p. 581-583.

31. Zhu, T., et al., *A Comparison of Scaffold Decomposition with Clustering Methods in Compound Set Enrichment to Identify Latent Chemical Series in High-Throughput Screening.*

32. Schrodinger, L., *Schrödinger Release 2023-3: LigPrep, Schrödinger, LLC, New York, NY, 2023.* 2023.

33. Epik, S., *Schrödinger Release 2023-3: Epik, Schrödinger, LLC, New York, NY, 2023.* 2023.

34. Shelley, J.C., et al., *Epik: a software program for pK a prediction and protonation state generation for drug-like molecules.* Journal of computer-aided molecular design, 2007. **21**: p. 681-691.

35. Dixon, S.L., et al., *PHASE: a new engine for pharmacophore perception, 3D QSAR model development, and 3D database screening: 1. Methodology and preliminary results.* Journal of computer-aided molecular design, 2006. **20**: p. 647-671.

36. Schrödinger, P., *Schrödinger Release 2023-3: Phase, Schrödinger, LLC, New York, NY, 2023.* 2023.

37. Yang, S.-Y., *Pharmacophore modeling and applications in drug discovery: challenges and recent advances.* Drug discovery today, 2010. **15**(11-12): p. 444-450.

38. Mysinger, M.M., et al., *Directory of useful decoys, enhanced (DUD-E): better ligands and decoys for better benchmarking.* Journal of medicinal chemistry, 2012. **55**(14): p. 6582-6594.

39. Ursu, O., et al., *DrugCentral: online drug compendium.* Nucleic acids research, 2016: p. gkw993.

40. Shivanyuk, A., et al., *Enamine real database: Making chemical diversity real.* Chemistry today, 2007. **25**(6): p. 58-59.

41. Schrödinger, P.P.W., *Schrödinger Release 2023-3: Protein Preparation Wizard; Epik, Schrödinger, LLC, New York, NY, 2023; Impact, Schrödinger, LLC, New York, NY; Prime, Schrödinger, LLC, New York, NY, 2023.* 2023.

42. Manual, U., *Schrödinger Release 2019−3: Glide, Schrödinger, LLC, New York, NY, 2019.* Schrödinger Release, 2018. **3**.

43. Friesner, R.A., et al., *Glide: a new approach for rapid, accurate docking and scoring. 1. Method and assessment of docking accuracy.* Journal of medicinal chemistry, 2004. **47**(7): p. 1739-1749.

44. Schrödinger, P., *Schrödinger Release 2023-3: Prime, Schrödinger, LLC, New York, NY, 2023.* 2023.

45. Jacobson, M.P., et al., *A hierarchical approach to all-atom protein loop prediction.* Proteins: Structure, Function, and Bioinformatics, 2004. **55**(2): p. 351-367.

46. Li, J., et al., *The VSGB 2.0 model: a next generation energy model for high resolution protein structure modeling.* Proteins: Structure, Function, and Bioinformatics, 2011. **79**(10): p. 2794-2812.

47. Lu, C., et al., *OPLS4: Improving force field accuracy on challenging regimes of chemical space.* Journal of chemical theory and computation, 2021. **17**(7): p. 4291-4300.

48. Genheden, S. and U. Ryde, *The MM/PBSA and MM/GBSA methods to estimate ligand-binding affinities.* Expert opinion on drug discovery, 2015. **10**(5): p. 449-461.

49. AlAjmi, M.F., et al., *Pharmacoinformatics approach for the identification of Polo-like kinase-1 inhibitors from natural sources as anti-cancer agents.* International journal of biological macromolecules, 2018. **116**: p. 173-181.

50. Release, S., *1: Desmond Molecular Dynamics System, DE Shaw Research, New York, NY, 2021. Maestro-Desmond Interoperability Tools, Schrödinger.* 2023.

51. Brańka, A., *Nosé-Hoover chain method for nonequilibrium molecular dynamics simulation.* Physical Review E, 2000. **61**(5): p. 4769.

52. Martyna, G.J., D.J. Tobias, and M.L. Klein, *Constant pressure molecular dynamics algorithms.* The Journal of chemical physics, 1994. **101**(5): p. 4177-4189.

53. Sadiq, S., et al., *Virtual screening of FDA-approved drugs against LasR of Pseudomonas aeruginosa for antibiofilm potential.* Molecules, 2020. **25**(16): p. 3723.

54. Ranganathan, S., K. Nakai, and C. Schonbach, *Encyclopedia of bioinformatics and computational biology: ABC of bioinformatics.* 2018: Elsevier.

55. Vuorinen, A. and D. Schuster, *Methods for generating and applying pharmacophore models as virtual screening filters and for bioactivity profiling.* Methods, 2015. **71**: p. 113-134.

56. Warren, G.L., et al., *A critical assessment of docking programs and scoring functions.* Journal of medicinal chemistry, 2006. **49**(20): p. 5912-5931.

57. Chen, H., et al., *On evaluating molecular-docking methods for pose prediction and enrichment factors.* Journal of chemical information and modeling, 2006. **46**(1): p. 401-415.

58. Kirchmair, J., et al., *Evaluation of the performance of 3D virtual screening protocols: RMSD comparisons, enrichment assessments, and decoy selection—what can we learn from earlier mistakes?* Journal of computer-aided molecular design, 2008. **22**: p. 213-228.

59. Truchon, J.-F. and C.I. Bayly, *Evaluating virtual screening methods: good and bad metrics for the "early recognition" problem.* Journal of chemical information and modeling, 2007. **47**(2): p. 488-508.

60. Triballeau, N., et al., *Virtual screening workflow development guided by the "receiver operating characteristic" curve approach. Application to high-throughput docking on metabotropic glutamate receptor subtype 4.* Journal of medicinal chemistry, 2005. **48**(7): p. 2534-2547.

61. Davis, A.M. and R.J. Riley, *Predictive ADMET studies, the challenges and the opportunities.* Current opinion in chemical biology, 2004. **8**(4): p. 378-386.

62. Jambhekar, S.S. and P.J. Breen, *Drug dissolution: significance of physicochemical properties and physiological conditions.* Drug Discovery Today, 2013. **18**(23-24): p. 1173-1184.

63. Meanwell, N.A., *Improving drug candidates by design: a focus on physicochemical properties as a means of improving compound disposition and safety.* Chemical research in toxicology, 2011. **24**(9):

p. 1420-1456.

64. Wu, Y., *An improved method for predicting logP.* 2006.

65. Varma, M., et al., *Extended Clearance Classification System (ECCS) informed approach for evaluating investigational drugs as substrates of drug transporters.* Clinical Pharmacology & Therapeutics, 2017. **102**(1): p. 33-36.

66. Savjani, K.T., A.K. Gajjar, and J.K. Savjani, *Drug solubility: importance and enhancement techniques.* International Scholarly Research Notices, 2012. **2012**.

67. Kallinteri, P. and S.G. Antimisiaris, *Solubility of drugs in the presence of gelatin: effect of drug lipophilicity and degree of ionization.* International journal of pharmaceutics, 2001. **221**(1-2): p. 219-226.

68. Kah, M. and C.D. Brown, *Log D: Lipophilicity for ionisable compounds.* Chemosphere, 2008. **72**(10): p. 1401-1408.

69. Zhang, Z. and W. Tang, *Drug metabolism in drug discovery and development.* Acta Pharmaceutica Sinica B, 2018. **8**(5): p. 721-732.

70. DeGorter, M., et al., *Drug transporters in drug efficacy and toxicity.* Annual review of pharmacology and toxicology, 2012. **52**: p. 249-273.

71. Arome, D. and E. Chinedu, *The importance of toxicity testing.* Journal of Pharmaceutical and BioSciences, 2013. **4**: p. 146-148.

72. Sui, X., et al., *Predicting the volume of distribution of drugs in humans.* Current drug metabolism, 2008. **9**(6): p. 574-580.

73. Parthsarathy, V., et al., *A novel retro-inverso peptide inhibitor reduces amyloid deposition, oxidation and inflammation and stimulates neurogenesis in the APPswe/PS1ΔE9 mouse model of Alzheimer's disease.* PLoS One, 2013. **8**(1): p. e54769.

74. Paroni, G., P. Bisceglia, and D. Seripa, *Understanding the amyloid hypothesis in Alzheimer's disease.* Journal of Alzheimer's Disease, 2019. **68**(2): p. 493-510.

75. Hussain, I., et al., *Identification of a novel aspartic protease (Asp 2) as β-secretase.* Molecular and Cellular Neuroscience, 1999. **14**(6): p. 419-427.

76. Pushpakom, S., et al., *Drug repurposing: progress, challenges and recommendations.* Nature reviews Drug discovery, 2019. **18**(1): p. 41-58.

77. Langedijk, J., et al., *Drug repositioning and repurposing: terminology and definitions in literature.* Drug discovery today, 2015. **20**(8): p. 1027-1034.

78. Pal, S., et al., *Ligand-based pharmacophore modeling, virtual screening and molecular docking studies for discovery of potential topoisomerase I inhibitors.* Computational and structural biotechnology journal, 2019. **17**: p. 291-310.

79. Kaur, P., V. Sharma, and V. Kumar, *Pharmacophore Modelling and 3D-QSAR Studies on N.* International journal of medicinal chemistry, 2012. **2012**.

80. Bhadoriya, K.S., M.C. Sharma, and S.V. Jain, *Pharmacophore modeling and atom-based 3D-QSAR studies on amino derivatives of indole as potent isoprenylcysteine carboxyl methyltransferase (lcmt) inhibitors.* Journal of Molecular Structure, 2015. **1081**: p. 466-476.

81. Li, Y., et al., *Pharmacophore modeling, molecular docking and molecular dynamics simulations toward identifying lead compounds for Chk1.* Computational Biology and Chemistry, 2018. **76**: p. 53-60.

82. Reddy, K.K., et al., *Pharmacophore modelling and atom-based 3D-QSAR studies on N-methyl pyrimidones as HIV-1 integrase inhibitors.* Journal of enzyme inhibition and medicinal chemistry, 2012. **27**(3): p. 339-347.

83. Xie, H., K. Qiu, and X. Xie, *Pharmacophore modeling, virtual screening, and 3D-QSAR studies on a series of non-steroidal aromatase inhibitors.* Medicinal Chemistry Research, 2015. **24**: p. 1901-1915.

84. Foudah, A.I., et al., *Optimization, pharmacophore modeling and 3D-QSAR studies of sipholanes as breast cancer migration and proliferation inhibitors.* European Journal of Medicinal Chemistry, 2014. **73**: p. 310-324.

85. Bhatia, M.S., et al., *Pharmacophore modeling and 3D QSAR studies of aryl amine derivatives as potential lumazine synthase inhibitors.* Arabian Journal of Chemistry, 2017. **10**: p. S100-S104.

86. Taha, M.O., et al., *Discovery of new MurF inhibitors via pharmacophore modeling and QSAR analysis followed by in-silico screening.* Bioorganic & medicinal chemistry, 2008. **16**(3): p. 1218-1235.

87. Ferreira, L.G., et al., *Molecular docking and structure-based drug design strategies.* Molecules, 2015. **20**(7): p. 13384-13421.

88. Salo-Ahen, O.M., et al., *Molecular dynamics simulations in drug discovery and pharmaceutical development.* Processes, 2020. **9**(1): p. 71.

89. Durrant, J.D. and J.A. McCammon, *Molecular dynamics simulations and drug discovery.* BMC biology, 2011. **9**(1): p. 1-9.

90. Daoud, N.E.-H., et al., *ADMET profiling in drug discovery and development: perspectives of in silico, in vitro and integrated approaches.* Current Drug Metabolism, 2021. **22**(7): p. 503-522.

Figures
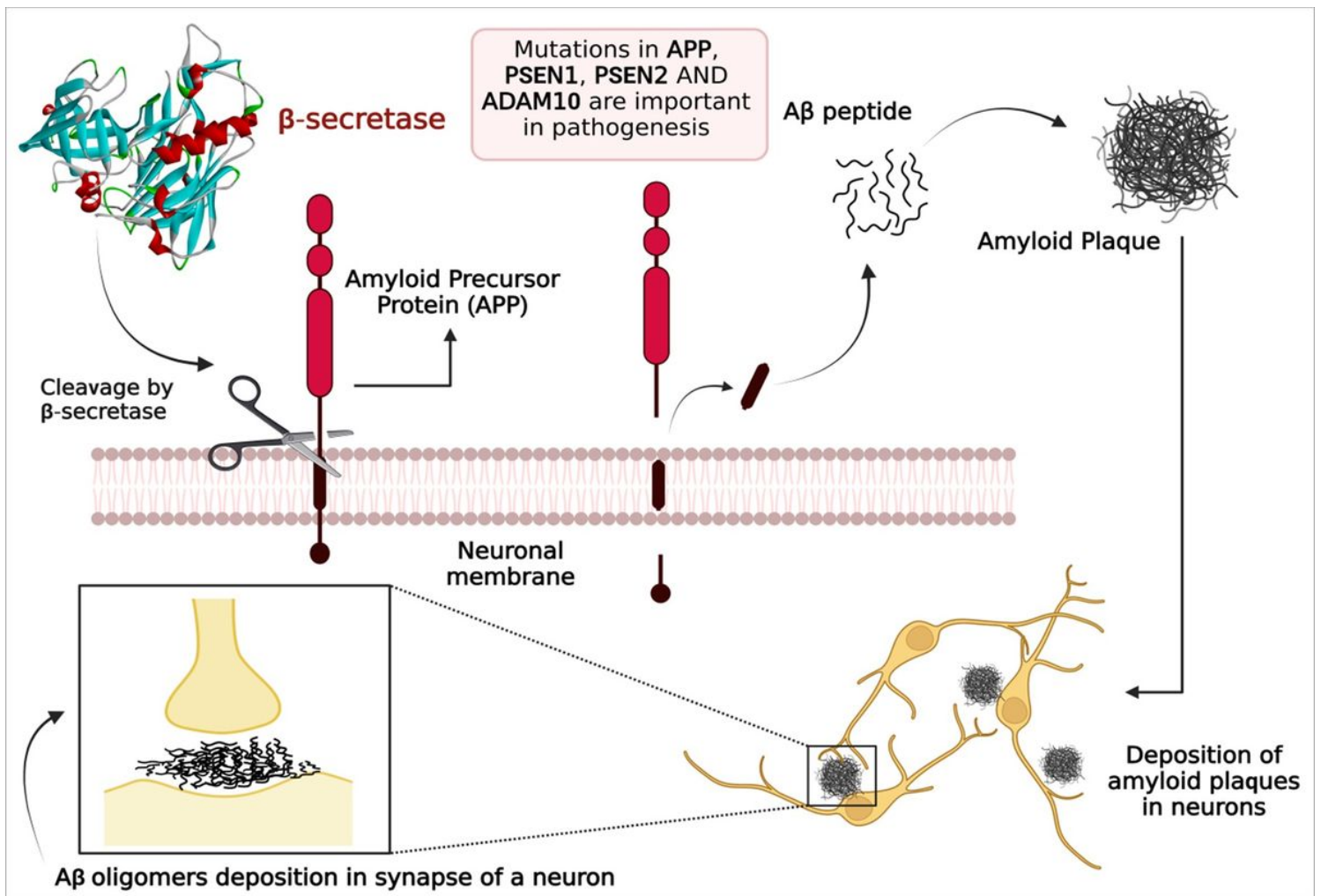
Figure 1

Canonical pathway for pathogenesis in Alzheimer's disease. Disruption in homeostasis leads to amyloid plaques as BACE-1 enzymes cleave the amyloid precursor protein to Aβ peptide, forming plaques deposited in the synaptic cleft.
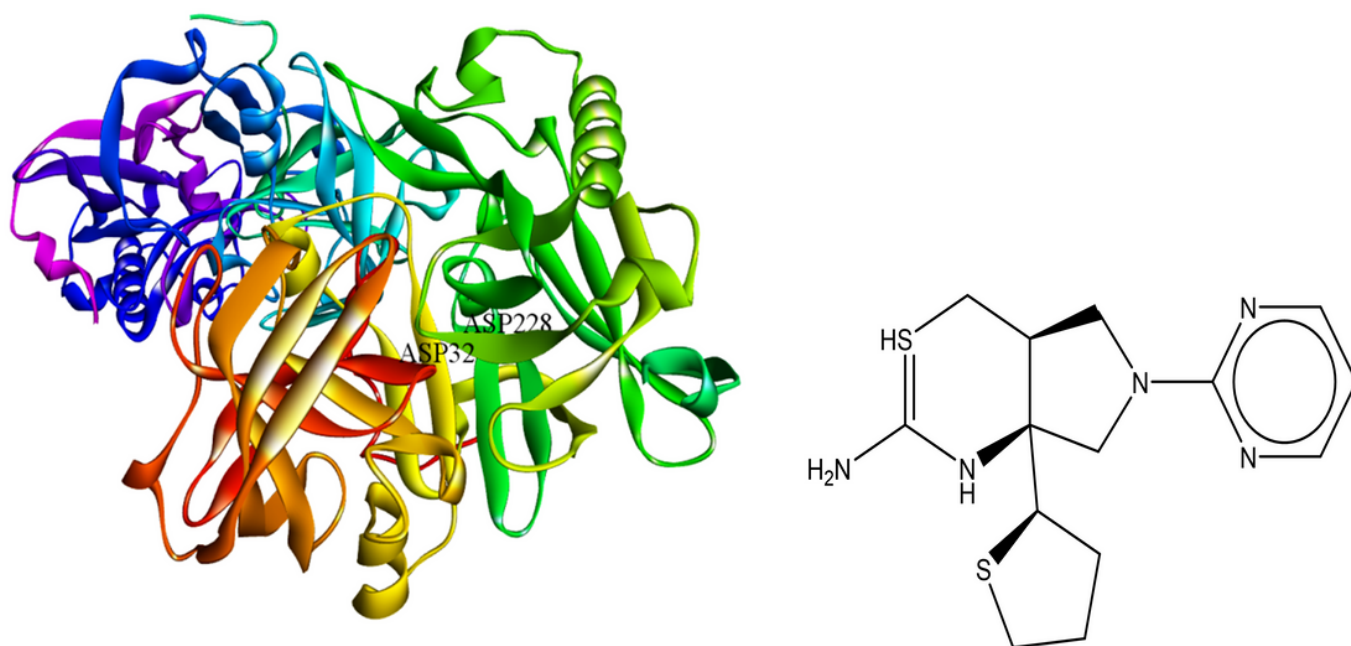
Figure 2

shows the 3D protein structure of human BACE-1 enzyme (PDB ID: 7MYI) with amino acids of the active site dyad labelled (ASP32 and ASP228). The chemical structure is the compound that is already docked to the active site of the protein 7MYI which was obtained from RCSB protein databank [24]
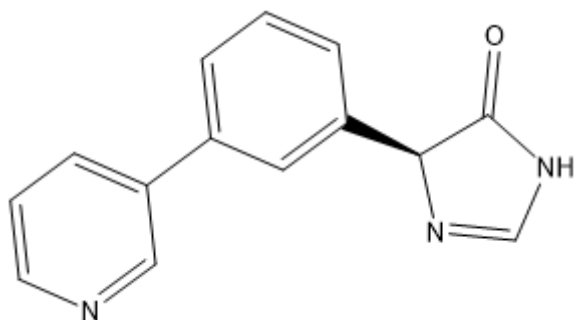
Figure 3

shows the common scaffold namely (S)-5-(3-(pyridin-3-yl)phenyl)-3,5-dihydro-4H-imidazol-4-on
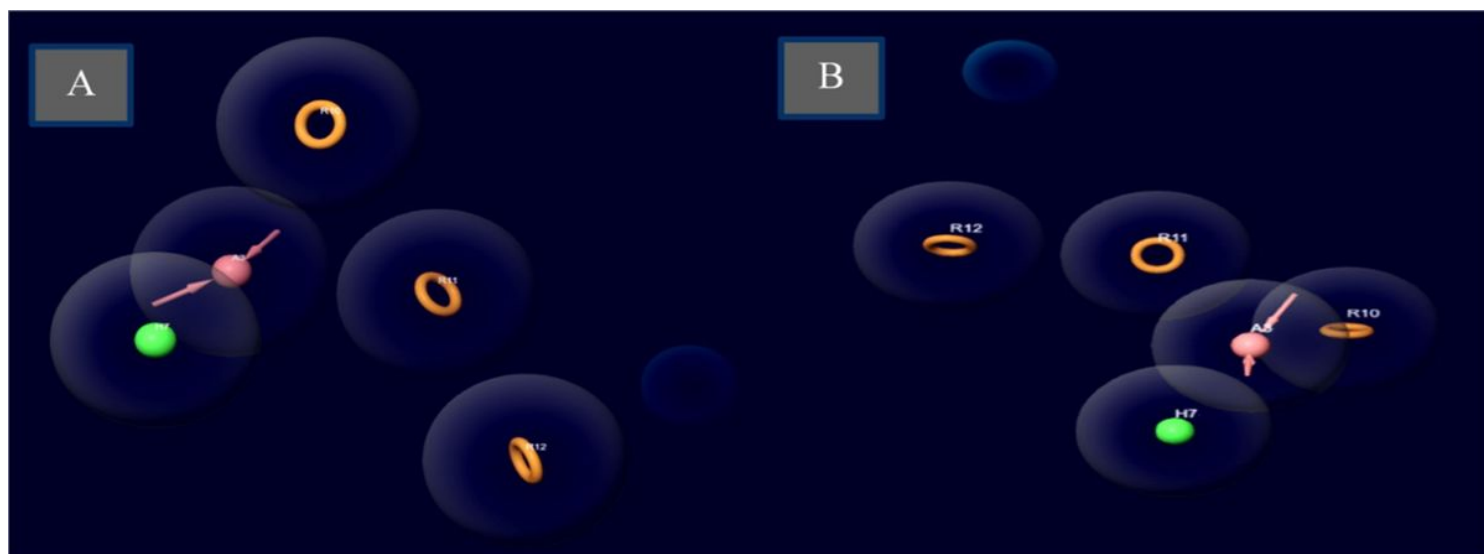
Figure 4

shows the pharmacophoric features of the chosen pharmacophore hypothesis (AHRRR). Five features illustrated as hydrogen bond acceptor (A3; pink), hydrophobic (H7; green) and aromatic rings (R10, R11, R12; orange). The model was generated by utilizing the known inhibitors of BACE-1 gathered from ChEMbL database. Part A and Part B of the figure show the pharmacophore hypothesis from two different angles.
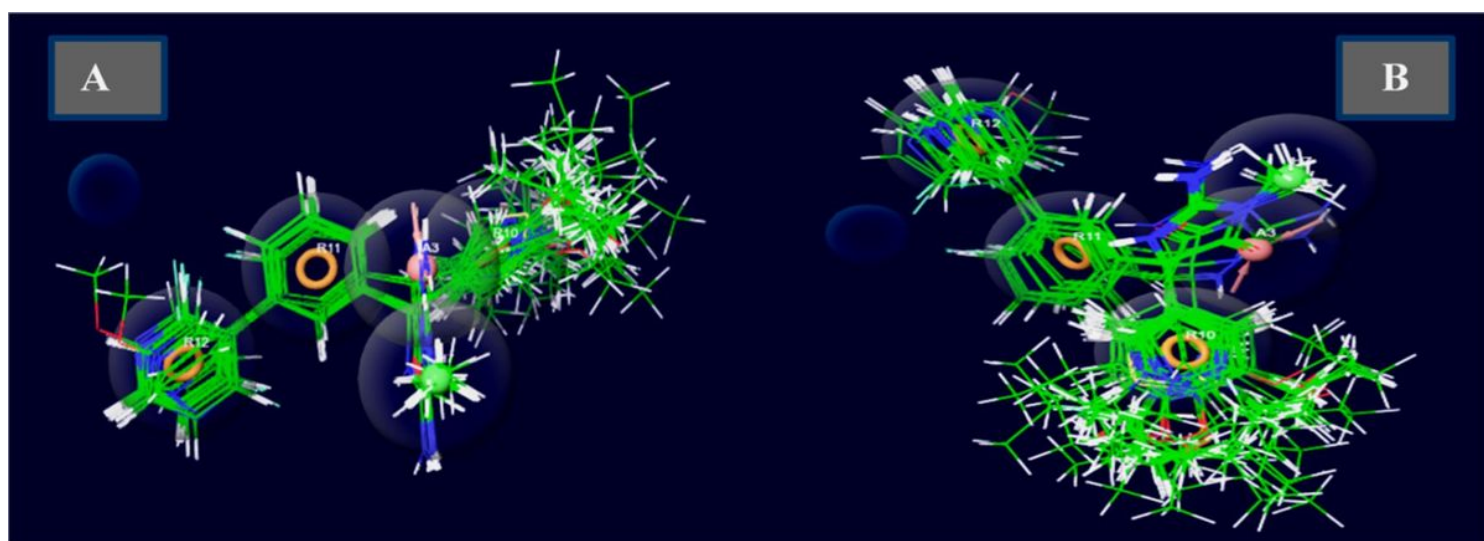
Figure 5

shows the active ligands superimposed with the hypothesis (AHRRR). This overlay graphic demonstrates the structural similarities of the active ligands with the hypothesis at hand.
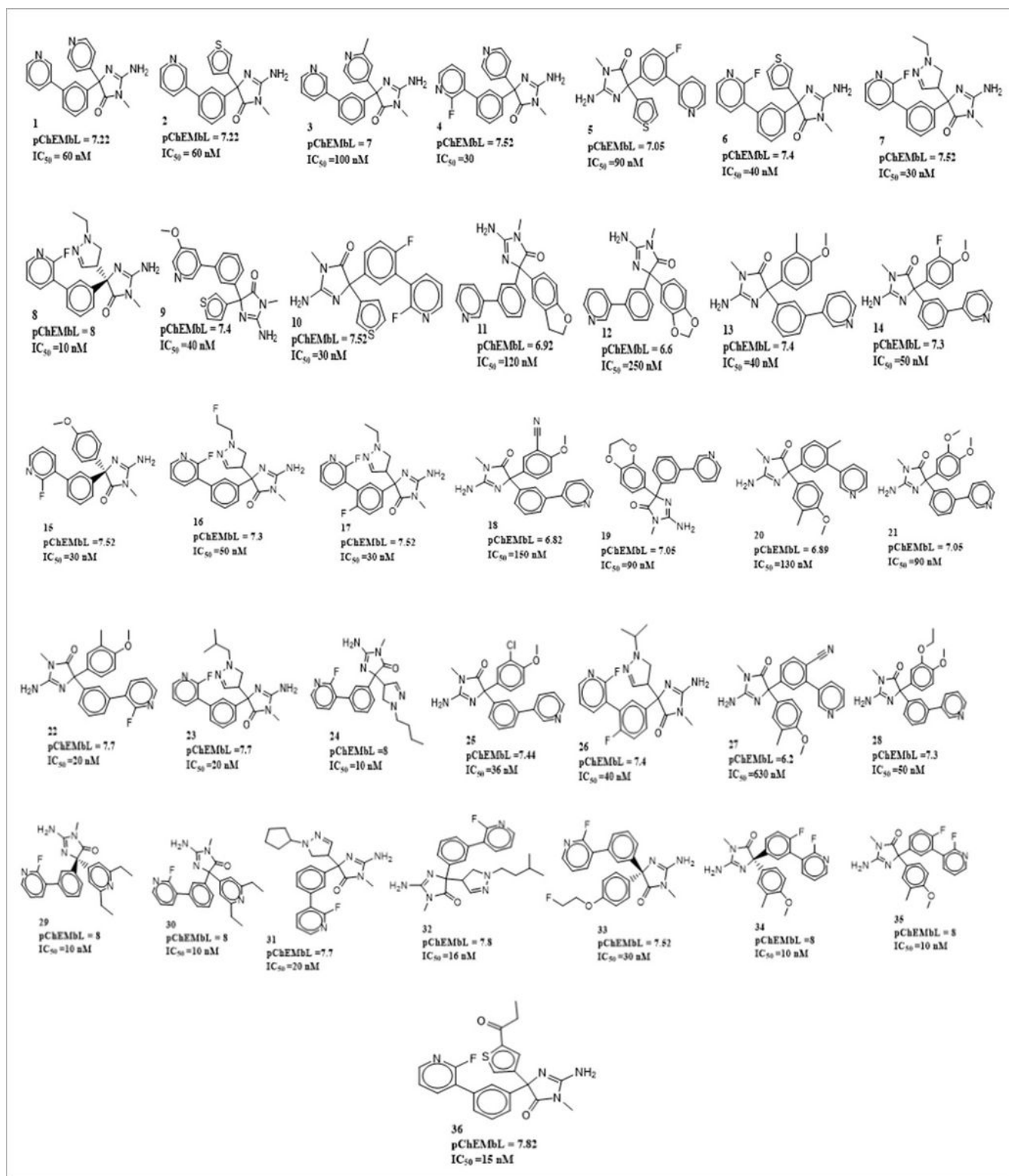
Figure 6

represents all the ligands in the training set that were used to generate the pharmacophore hypotheses. The figure also represents the code for the ligands, their IC_{50} values and pChEMbL values.
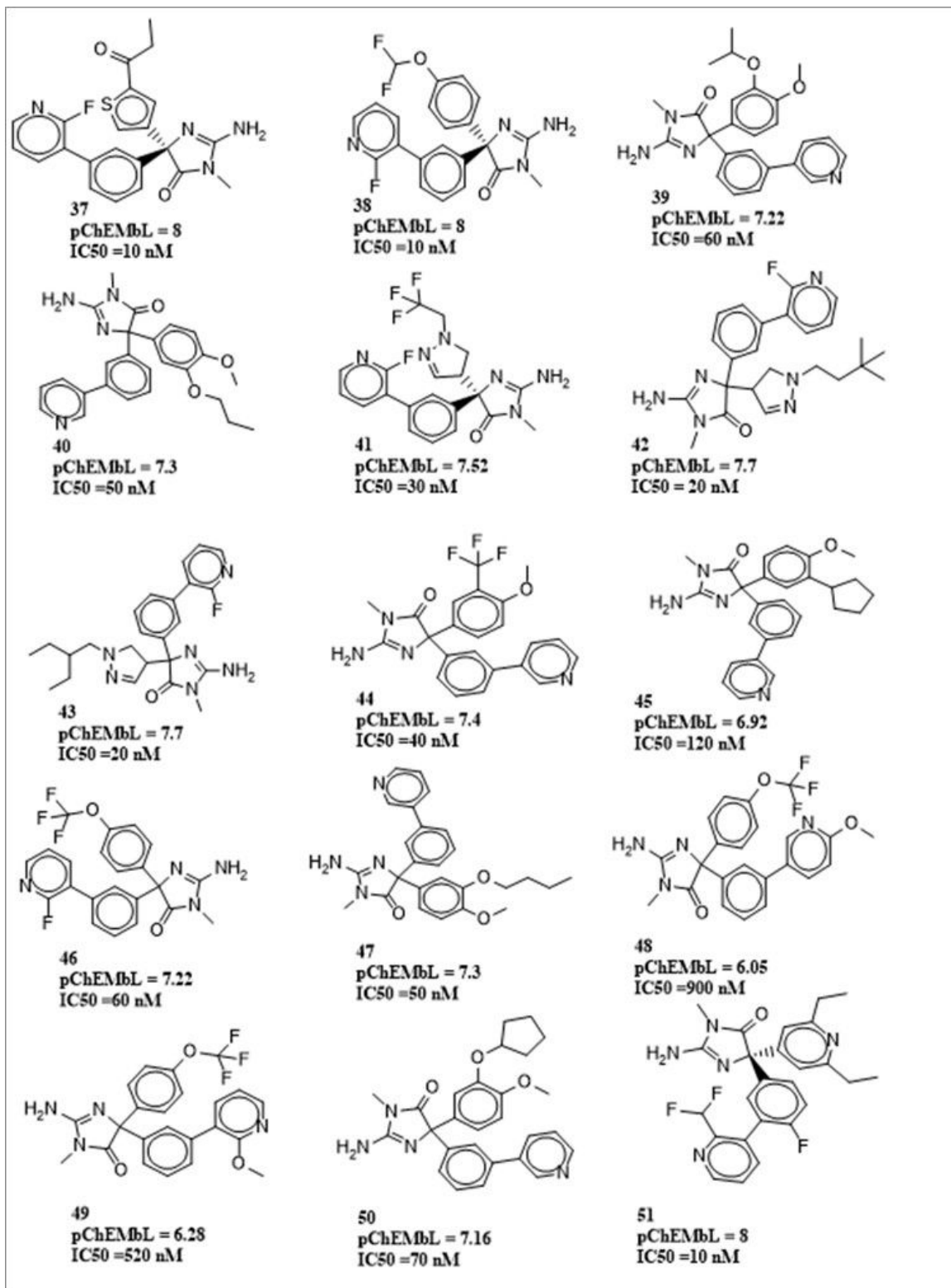
Figure 7

represents all the compounds in the active set that were used for the validation of pharmacophore hypothesis. The figure also represents the compound code, IC_{50} and pChEMbL values for all the compounds.
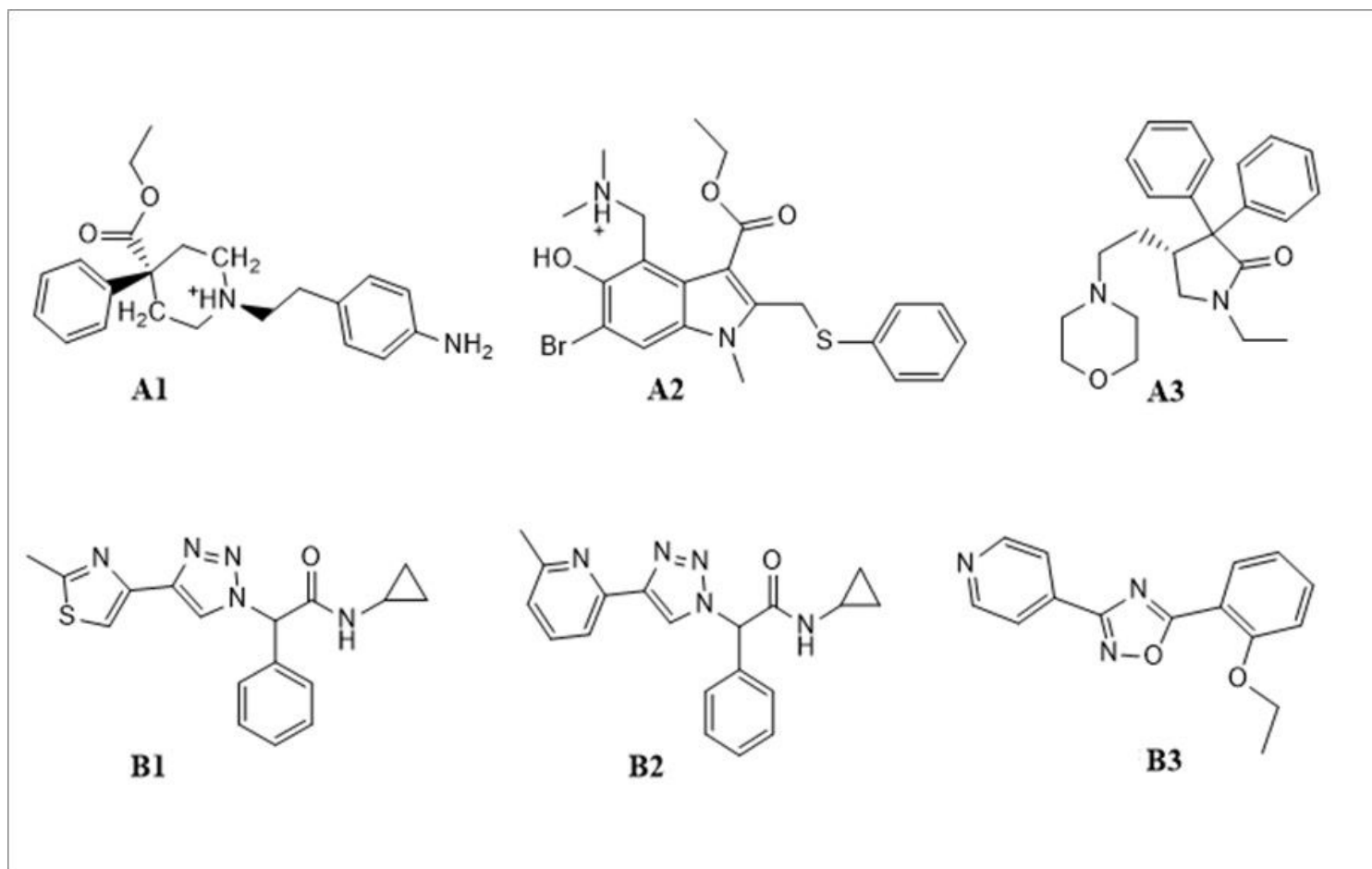
Figure 8

shows the chemical structures of the Hit molecules obtained after the screening of databases.
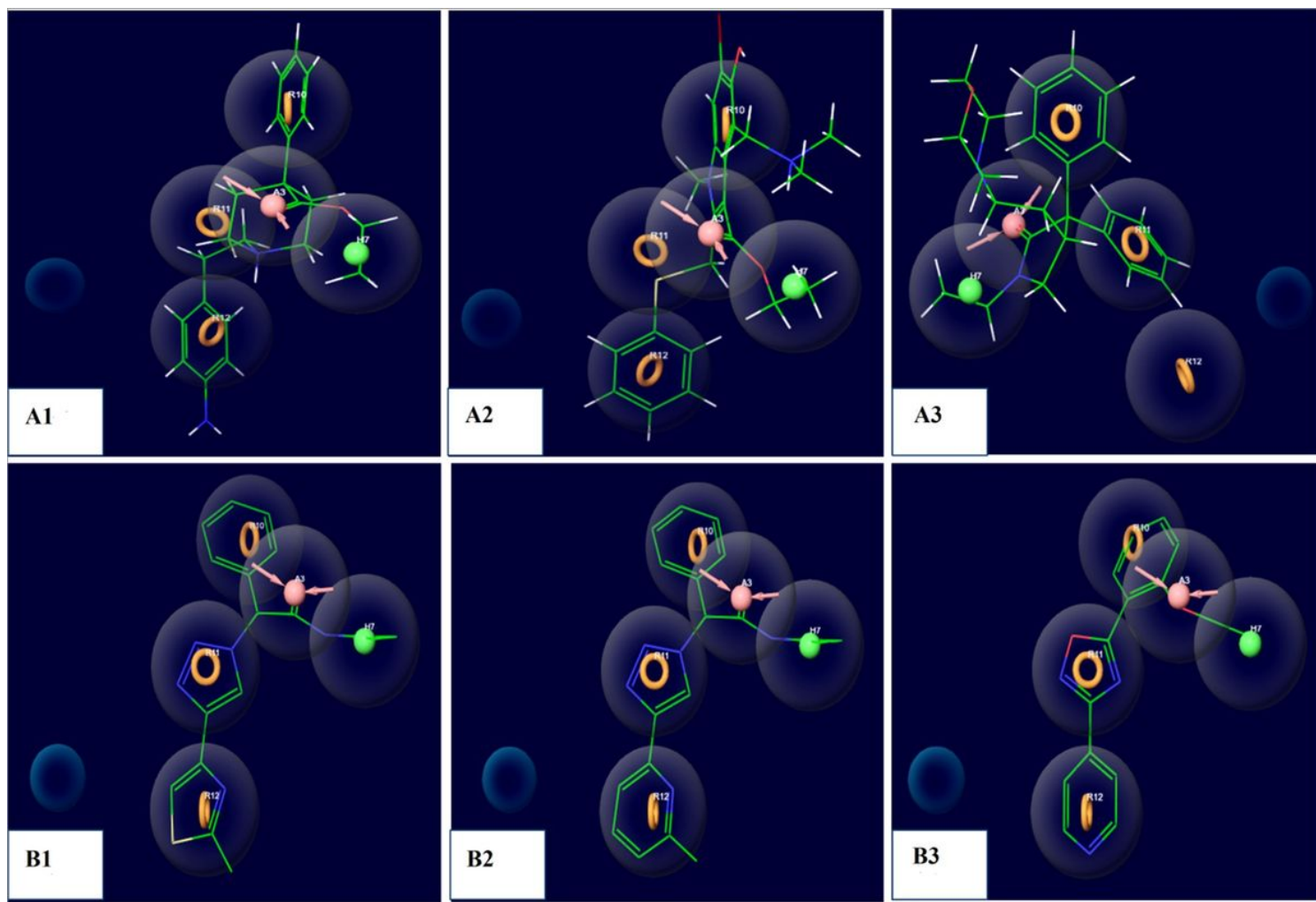
Figure 9

indicates the superimposed images of the screened hit molecules from the said databases with the selected pharmacophore hypothesis (AHRRR).

Figure 10

shows the 2D and 3D interactions of compound 6 (co-crystallized ligand) with protein 7MYI. The ligand was re-docked using GLIDE module of Schrodinger.
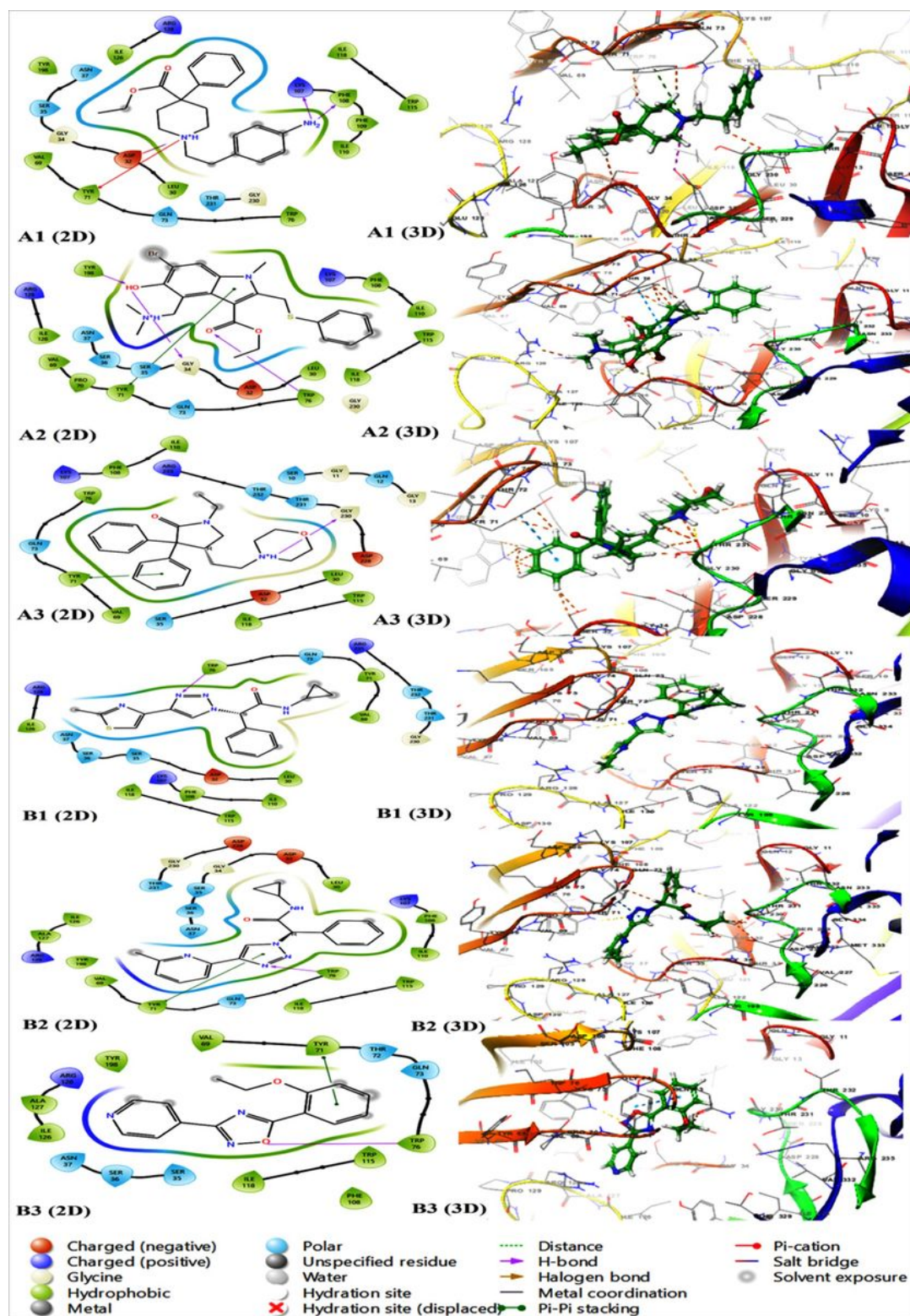
Figure 11

represents the docking interaction diagrams (2D and 3D) for all the Hit molecules (A1, A2, A3, B1, B2 and B3). Figure also shows that A1 has the interaction with amino acid residues that are common with the reference inhibitors and compound 6. The 3D picture also represents that the orientation of A1 is also similar to the reference inhibitors.
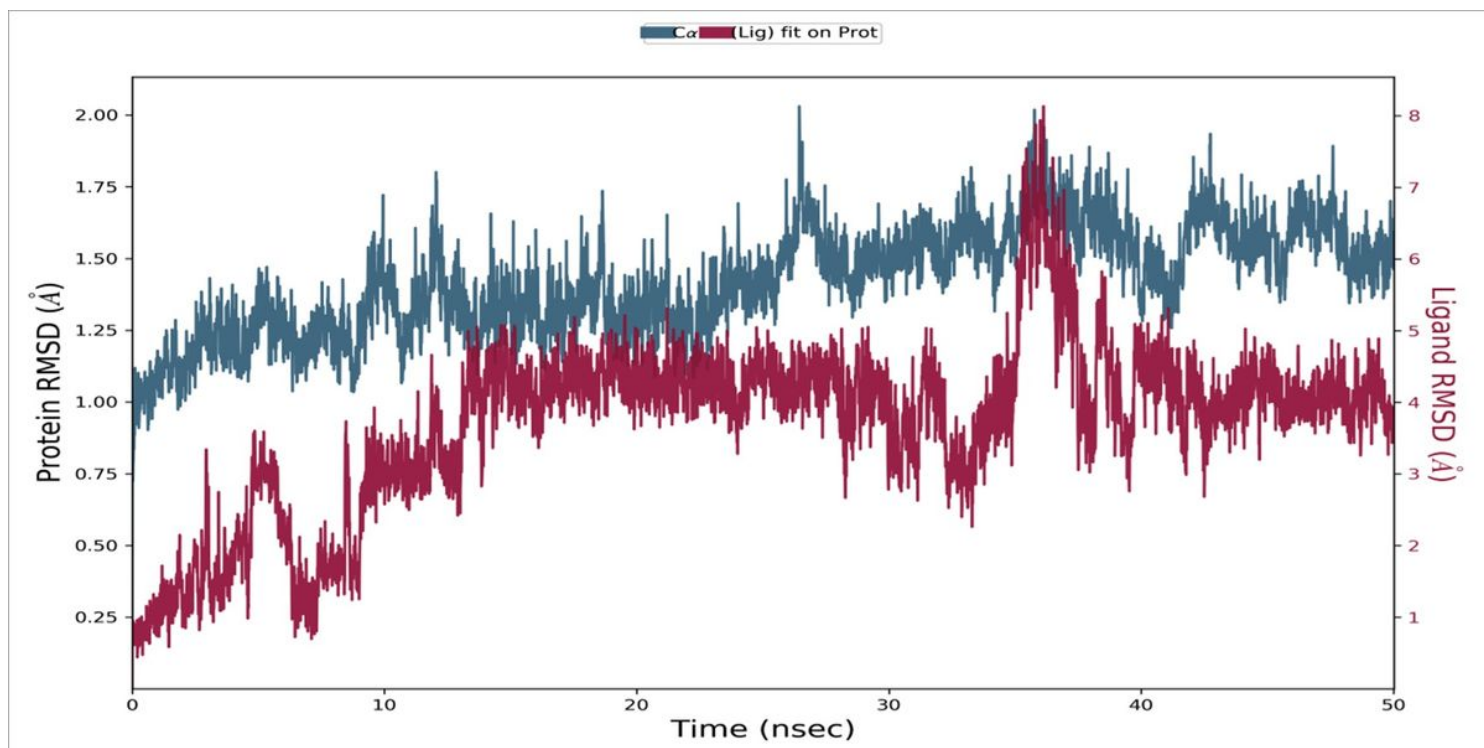
Figure 12

Shows RMSD trajectories obtained from MD simulation of anileridine-BACE-1 complex and the Apo form (no ligand)
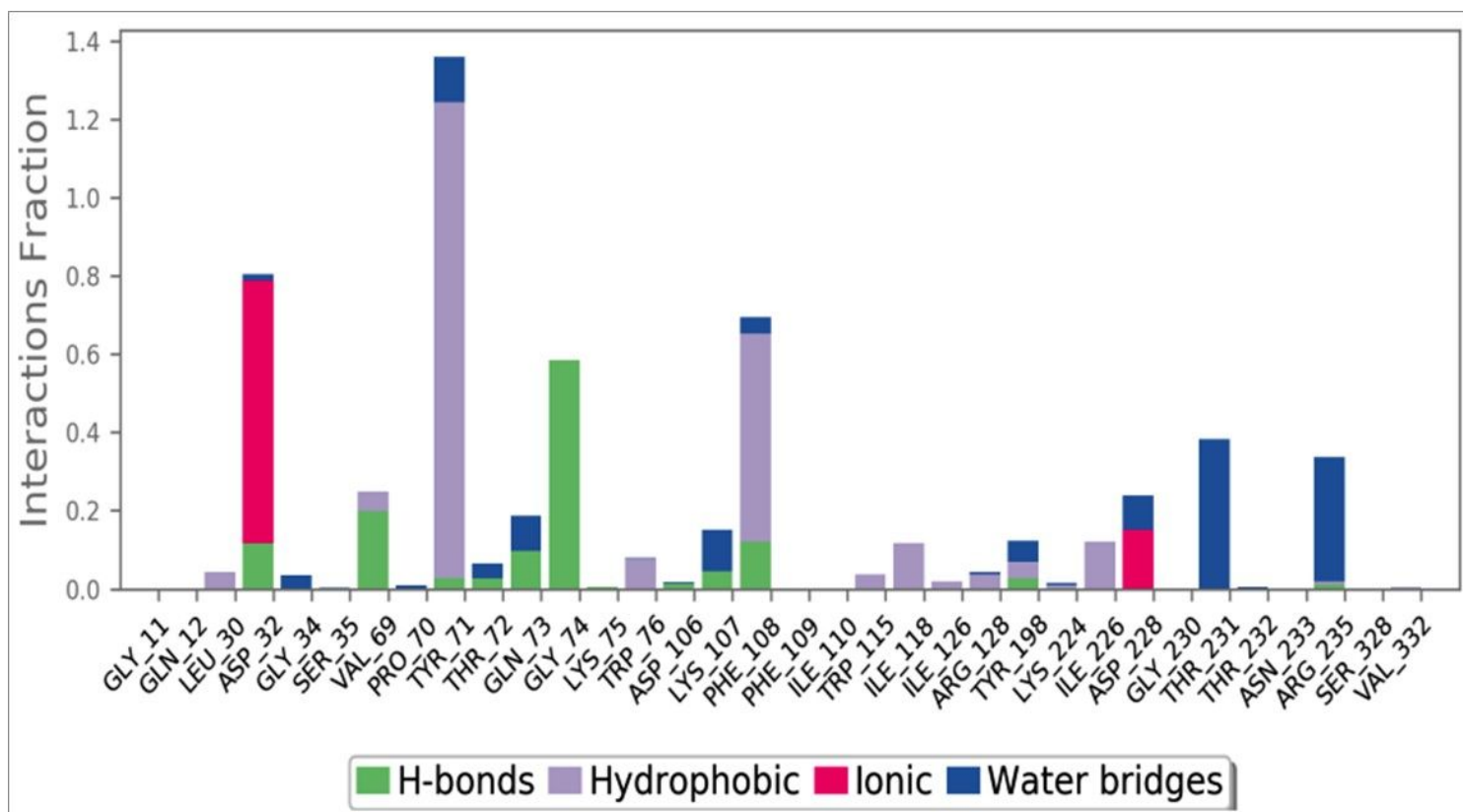
Figure 13

shows ligand-protein interactions duration during simulation. The figure depicts the interaction fraction of greater than 0.6 for Asp32, Tyr71, Phe108 and Gly74 along with an interaction fraction of between 0.3-0.4 for Thr231, Asp228 and Arg235.
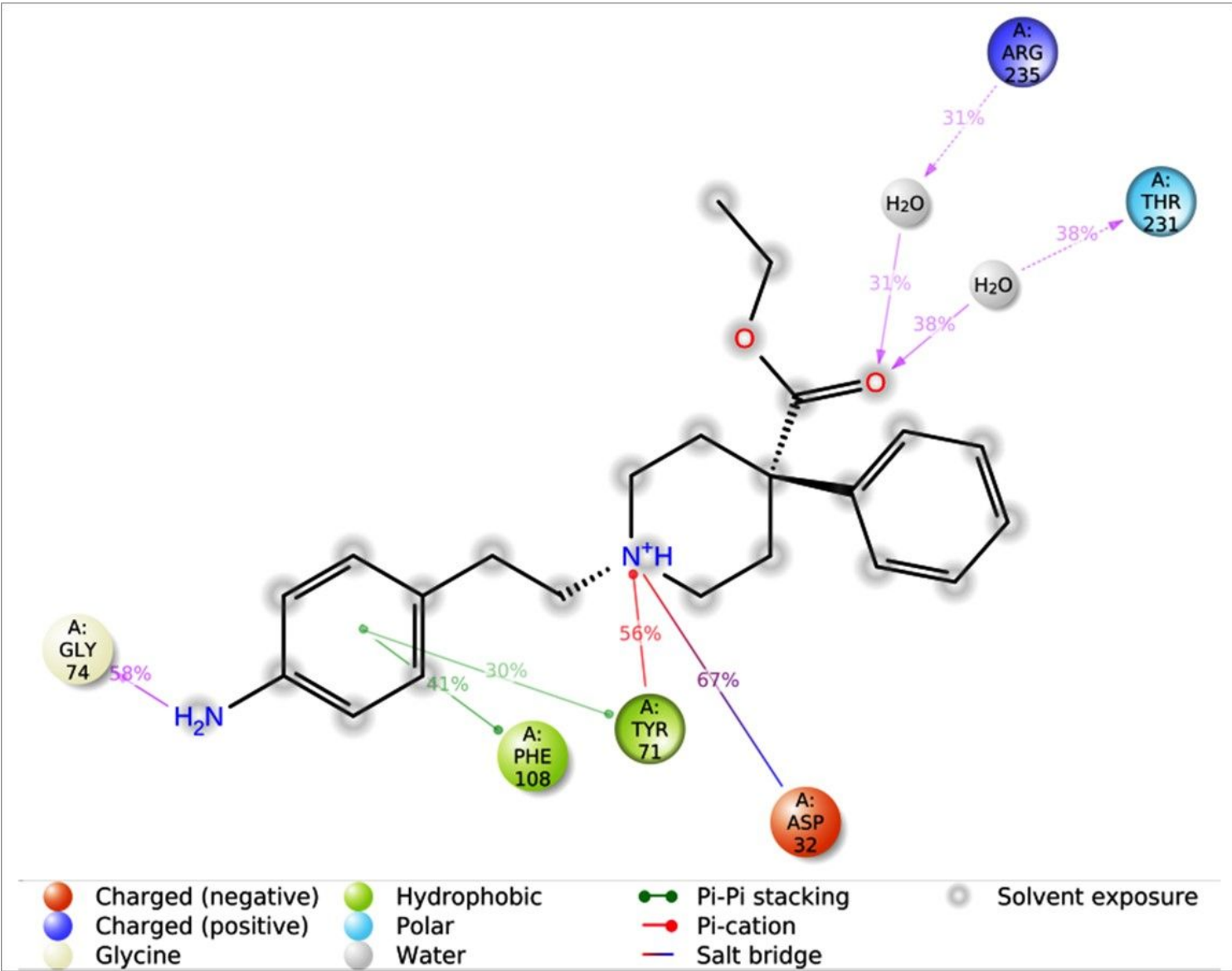
Figure 14

shows the atomic contribution in ligand protein interactions. One noticeable point is that there were no interaction observed in the docked complex with Thr231 and Arg235 but due to presence of water molecules they formed water bridges and formed an in-direct interaction the oxygen atom of the ligand molecule.
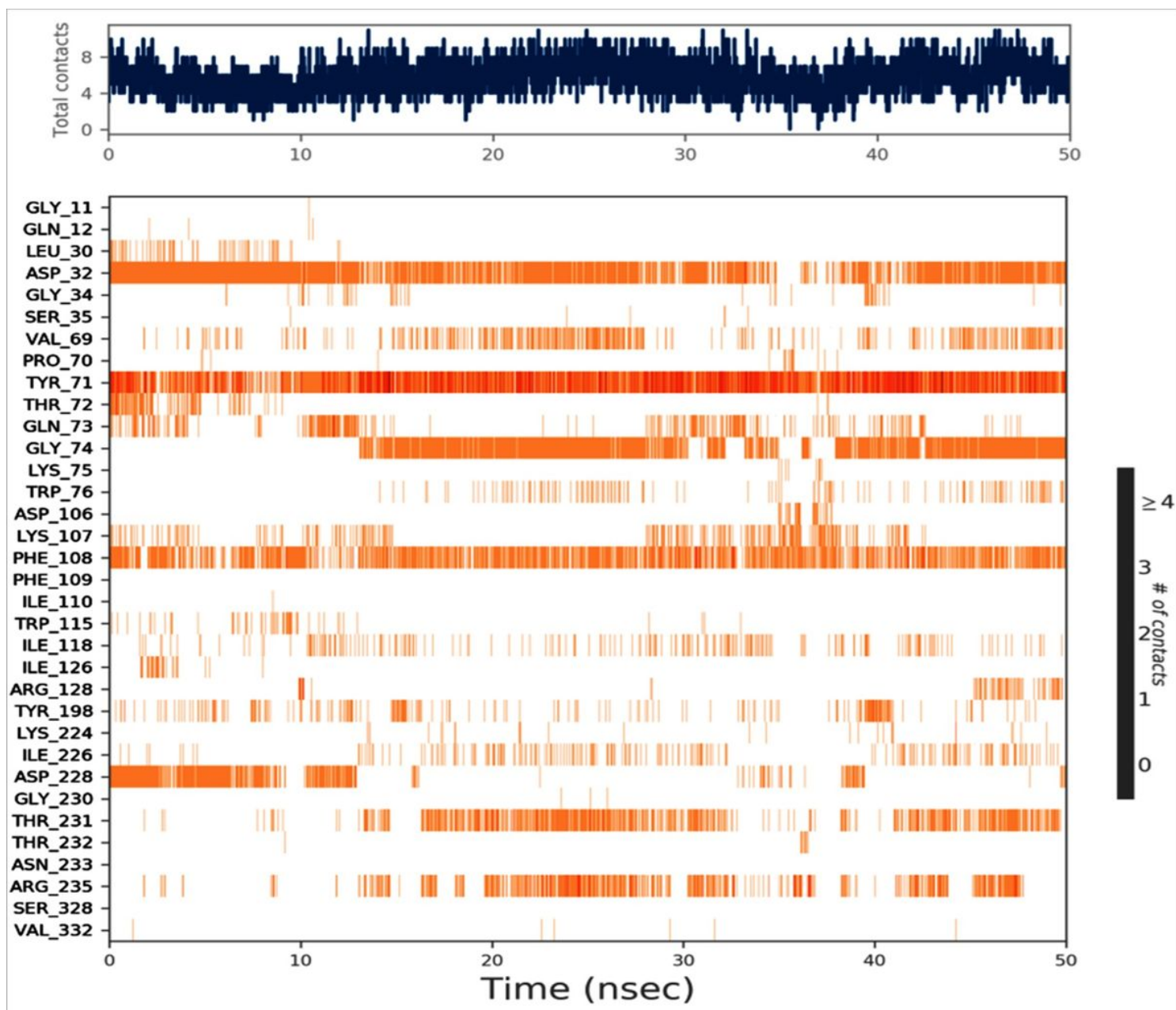
Figure 15

shows the total time of simulation on x-axis and amino acid interaction with the ligand on y-axis.
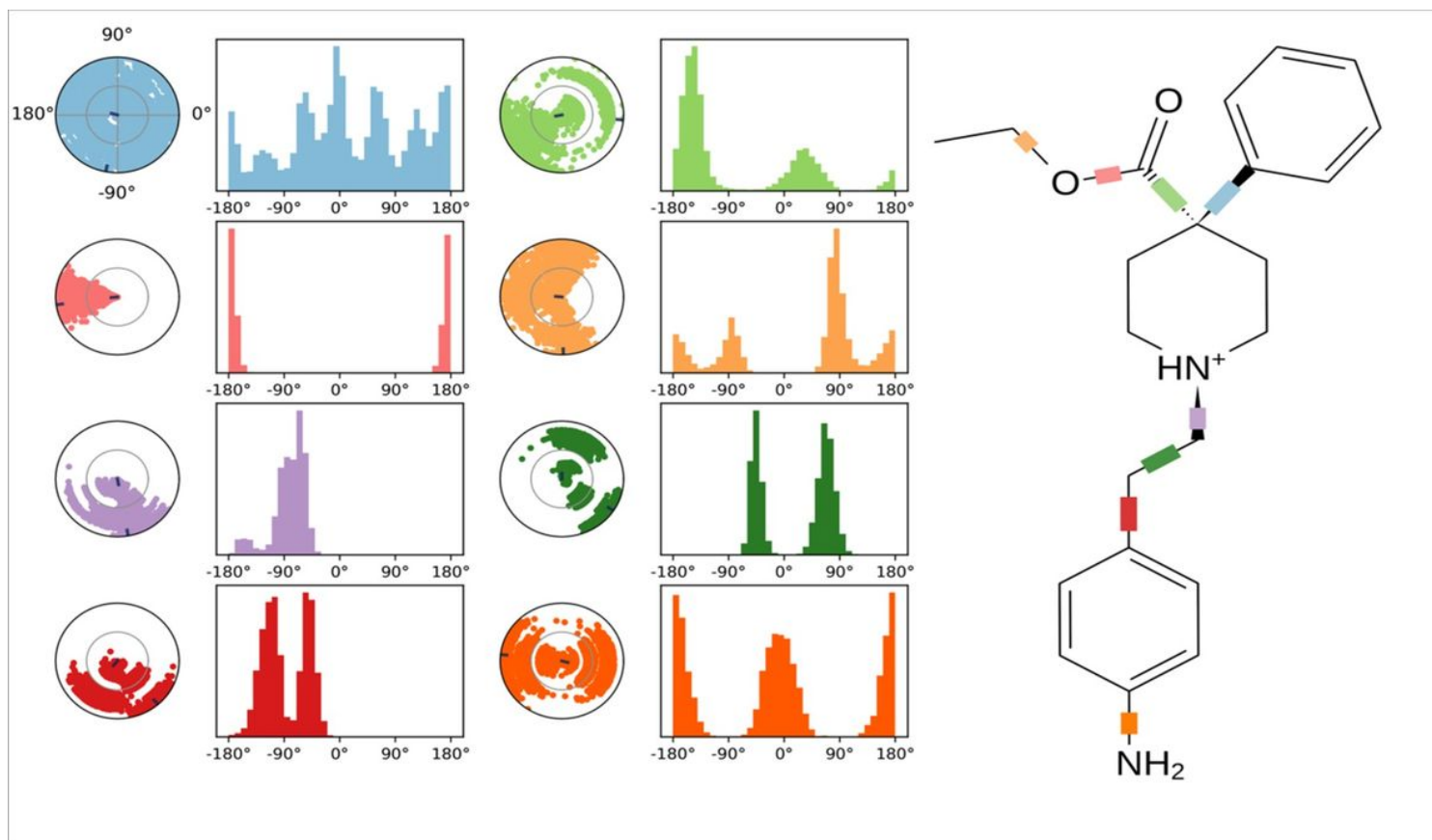
Figure 16

shows the torsional profile of Anileridine obtained via MD simulations. The torsional profile gives information about the rotatable bonds present in the ligand. The graph and 2D ligand shows the number of rotatable bonds in the present ligand and the degree of freedom and energy consumed as well. The potential values of the rotatable bonds are shown on the y-axis of the bar plot and are given in kcal/mol. The conformational strain the ligand experiences to retain a protein-bound shape can be understood by examining the correlations between the histogram and torsion potential.
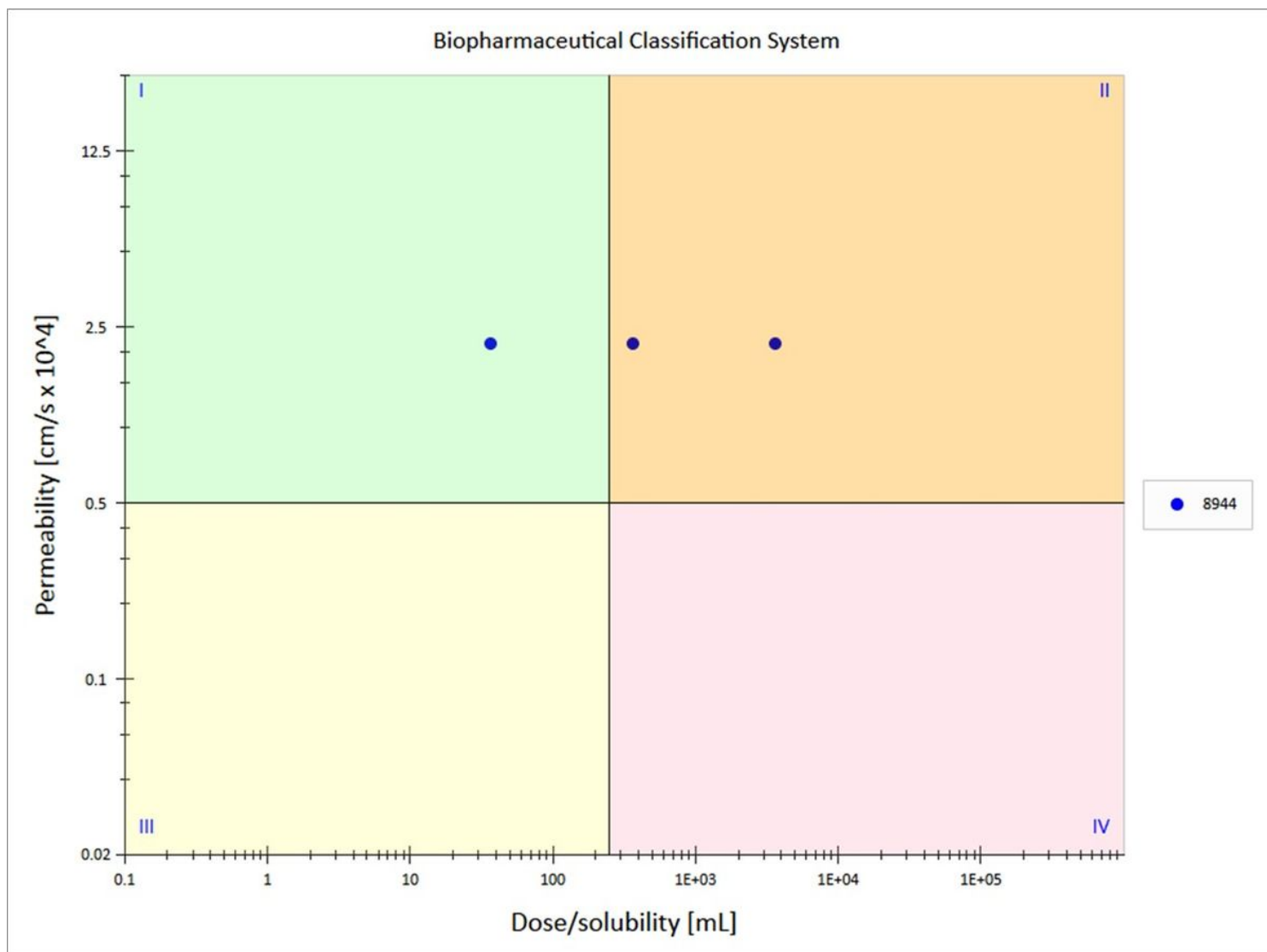
Figure 17

shows the BCS class of Anileridine. While calculating the BCS class the criteria set was S+Peff for permeability and intrinsic solubility for solubility parameter. The figure depicts that at doses 5mg, 50mg and 500mg the solubility and permeability of the drug remains at 0.131mg/ml and 2.237 cm/s x 10^4. The figure also shows that when increasing the dose of the drug the solubility profile of the drug decreases while permeability profile remains same.
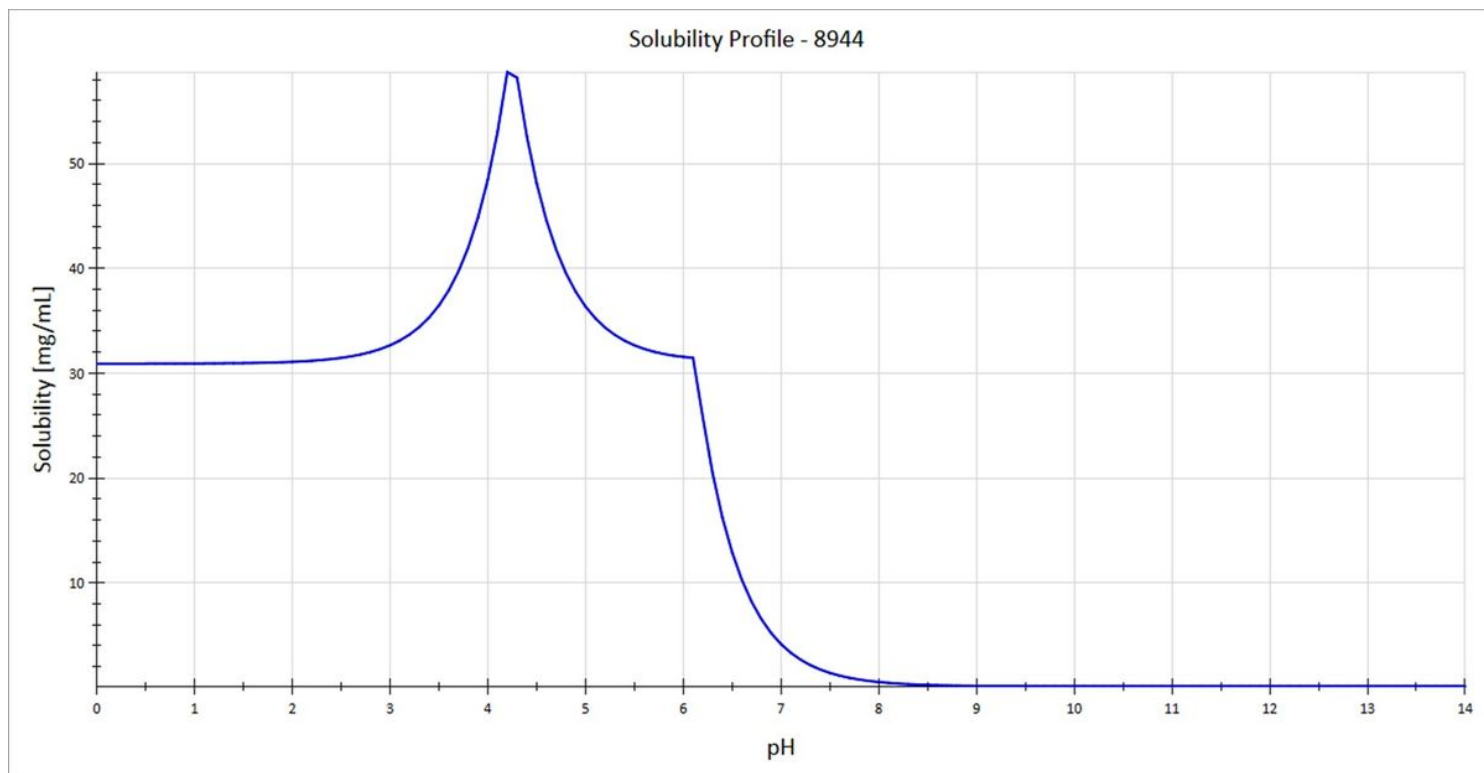
Solubility Profile - 8944

Figure 18

represents the solubility profile of anileridine with respect to changing pH.
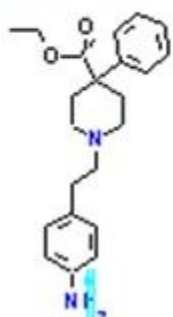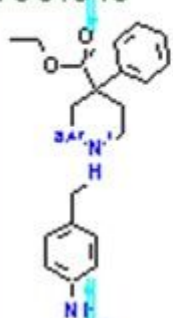
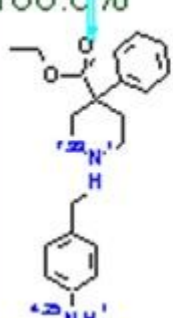| pKa	Macrostates	
	M	100.0%
8.47	HM⁺	8.47. 100.0%
4.25	H₂M⁺²	4.25. 100.0%

Figure 19

shows the microstates and pKa values for the drug. The microconstants are shown in red.
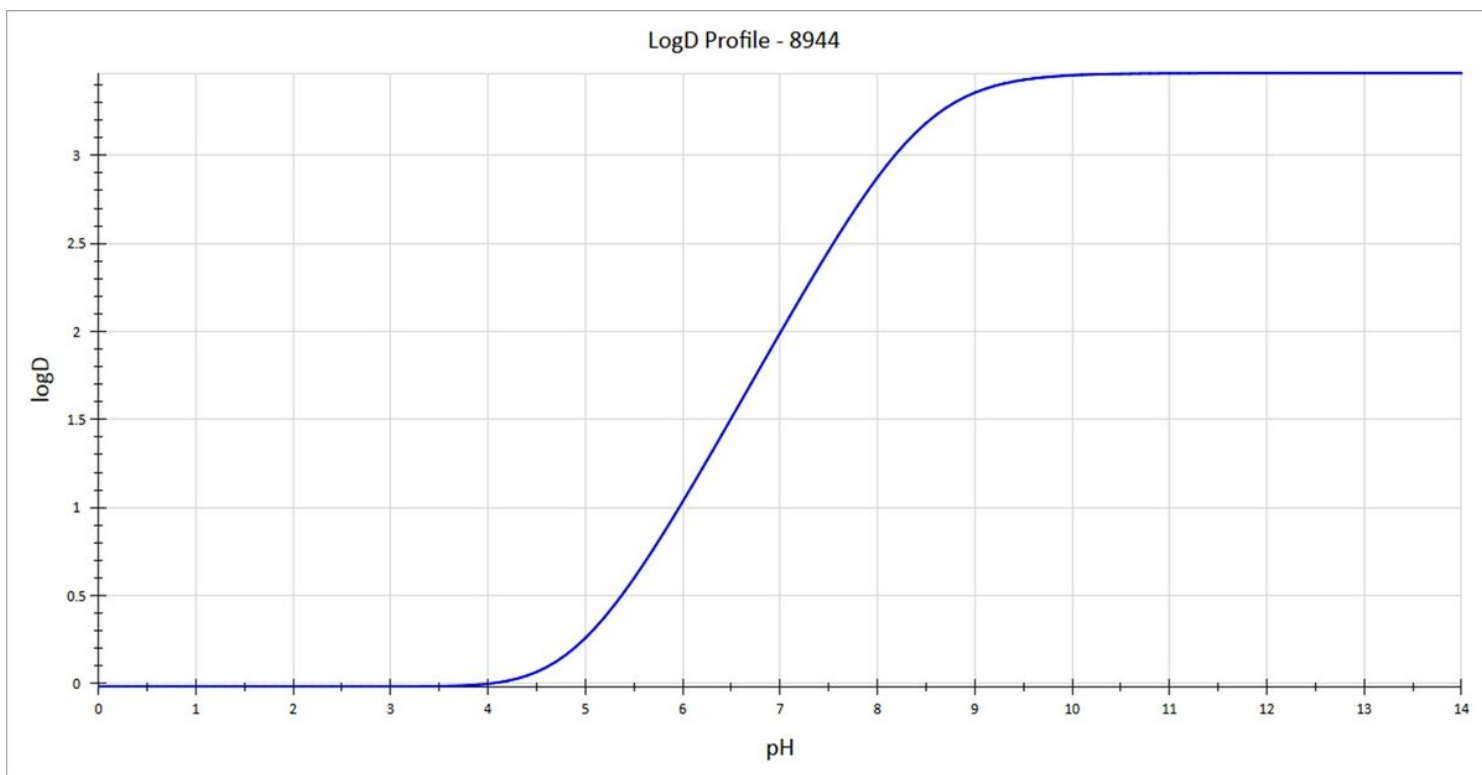
LogD Profile - 8944

Figure 20

shows the LogD profile in relation to pH.

CYP2C8_Sites of Metabolism

CYP2D6_Sites of Metabolism

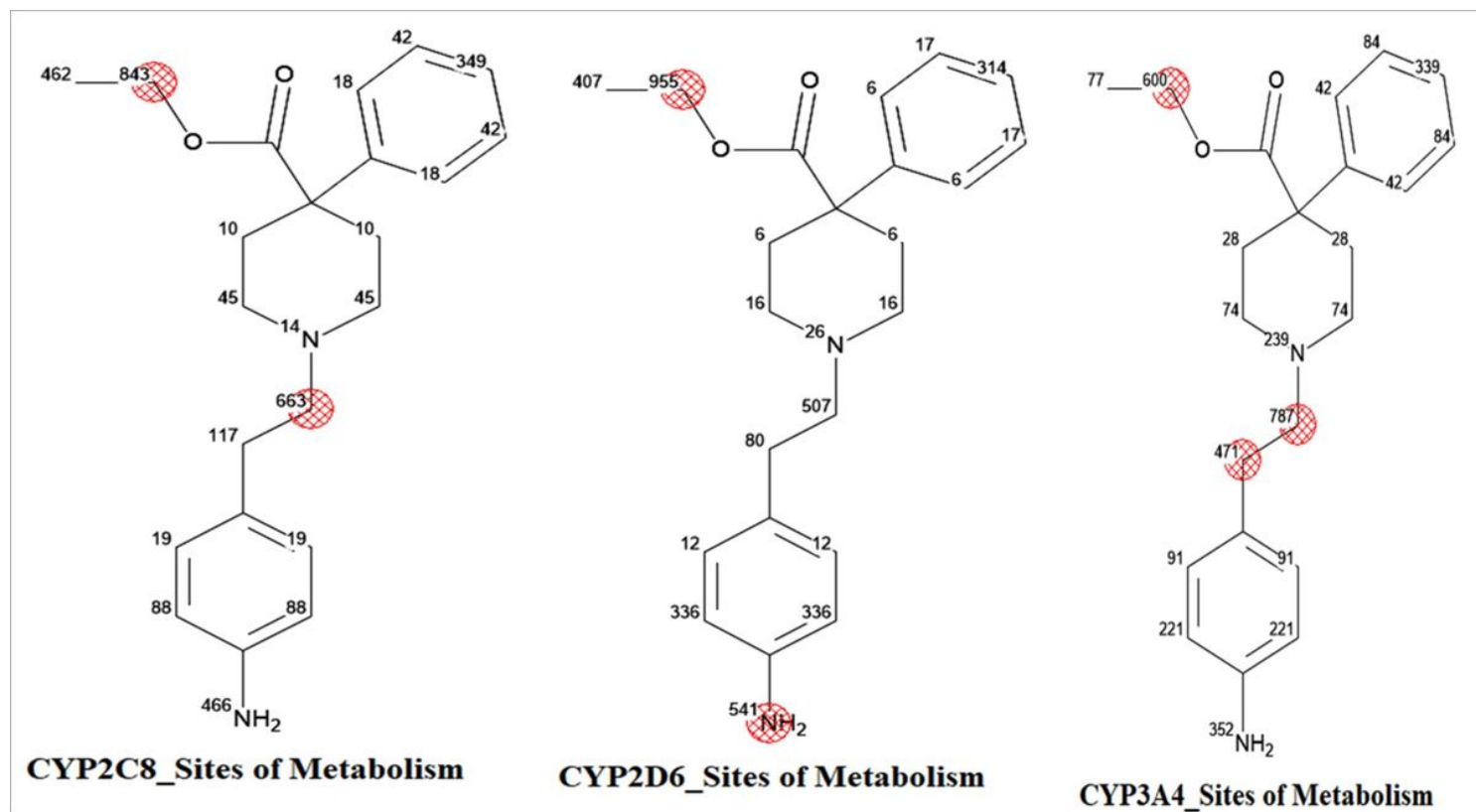CYP3A4_Sites of Metabolism

Figure 21

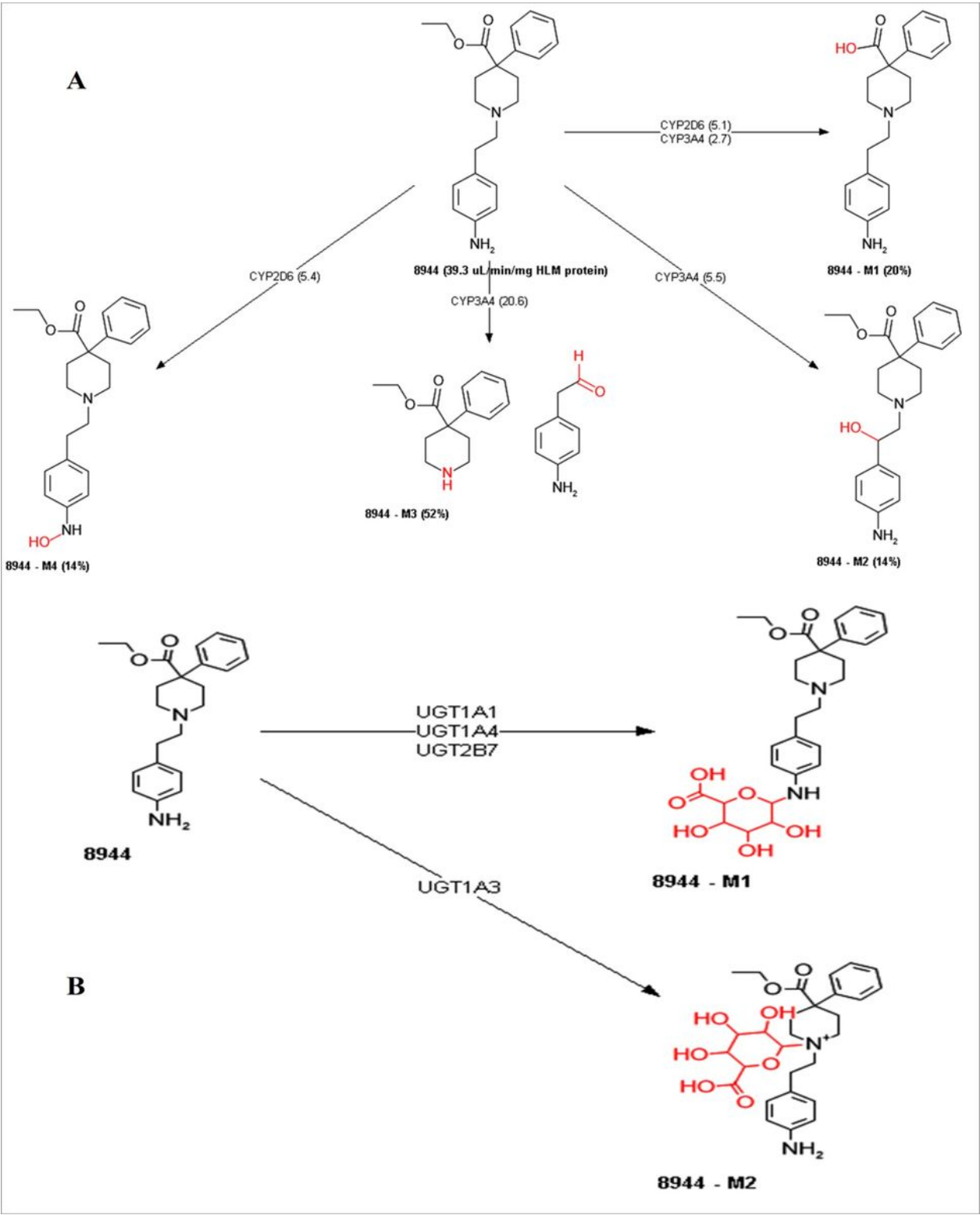represents the major CYP450 enzymes and their sites of metabolism. The sites of metabolism are labelled with red circles.

Figure 22

depicts all the metabolites and enzymes involved in the metabolism of anileridine along with percentages of each metabolite.
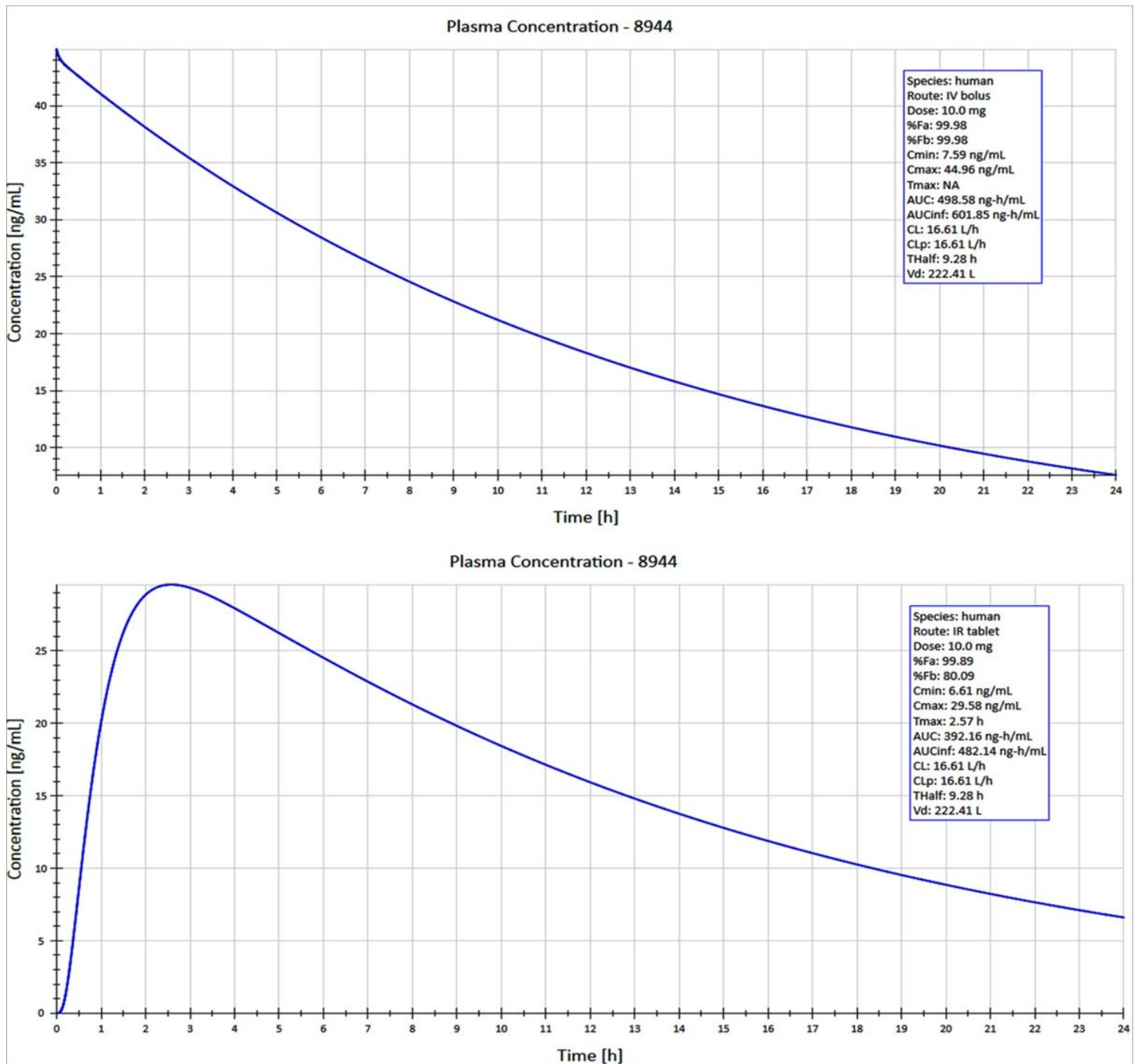
Plasma Concentration - 8944

Species: human
Route: IV bolus
Dose: 10.0 mg
%Fa: 99.98
%Fb: 99.98
Cmin: 7.59 ng/mL
Cmax: 44.96 ng/mL
Tmax: NA
AUC: 498.58 ng-h/mL
AUCinf: 601.85 ng-h/mL
CL: 16.61 L/h
CLp: 16.61 L/h
THalf: 9.28 h
Vd: 222.41 L

Plasma Concentration - 8944

Species: human
Route: IR tablet
Dose: 10.0 mg
%Fa: 99.89
%Fb: 80.09
Cmin: 6.61 ng/mL
Cmax: 29.58 ng/mL
Tmax: 2.57 h
AUC: 392.16 ng-h/mL
AUCinf: 482.14 ng-h/mL
CL: 16.61 L/h
CLp: 16.61 L/h
THalf: 9.28 h
Vd: 222.41 L

Figure 23

shows the simulated pharmacokinetic and biopharmaceutical parameters when 10mg of drug was given via both IV and oral route
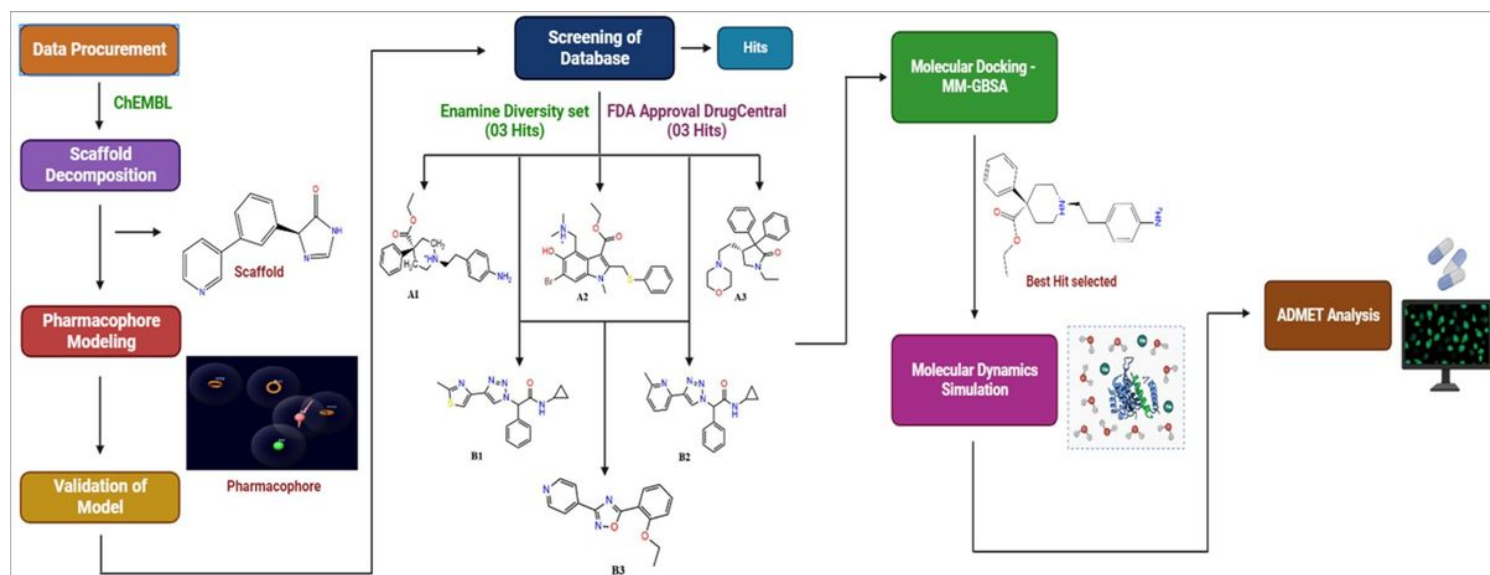
Figure 24

Graphical abstract represents the sequence of steps followed in the study and also showing the hit compounds obtained during the screening process.